3-25-2010

Residual Stress Analysis in 3C-SiC Thin Films by Substrate Curvature Method

Jose M. Carballo
University of South Florida

Residual Stress Analysis in 3C-SiC Thin Films by Substrate Curvature Method

by

Jose M. Carballo

A thesis submitted in partial fulfillment
of the requirements for the degree of
Master of Science in Mechanical Engineering
Department of Mechanical Engineering
College of Engineering
University of South Florida

Major Professor: Alex A. Volinsky, Ph.D.
Jose L. F. Porteiro, Ph.D.
Craig Lusk, Ph.D.

Date of Approval:
March 25, 2010

Keywords: stress analysis, Stoney's equation
curvature analysis, regularization, noise reduction

Dedication

I give thanks to my parents, brother, girlfriend, and friends for their constant support throughout my Master's program. Without their presence, I would have been greatly dispirited while completing this work.

Acknowledgements

I am thankful to Dr. Volinsky for his constant teaching attitude, support and motivation throughout this year. Also, special thanks to Dr. Saddow, and Chris Locke, for their contribution on samples for this work; and Richard Everly, N.N.R.C. staff, for his help on using the tools I needed. I also give thanks to my committee members, Dr. Porteiro and Dr. Lusk, and my group members, for their attention, and contribution to my work.

Table of Contents

List of Tables

List of Figures

Residual Stress Analysis in 3C-SiC Thin Films by
Substrate Curvature Method

Jose M. Carballo

ABSTRACT

Development of thin films has allowed for important improvements in optical, electronic and electromechanical devices within micrometer length scales. In order to grow thin films, there exist a wide variety of deposition techniques, as each technique offers a unique set of advantages. The main challenge of thin film deposition is to reach smallest possible dimensions, while achieving mechanical stability during operating conditions (including extreme temperatures and external forces, complex film structures and device configurations). Silicon carbide (SiC) is attractive for its resistance to harsh environments, and the potential it offers to improve performance in several microelectronic, micro-electromechanical, and optoelectronic applications. The challenge is to overcome presence of high defect densities within structure of SiC while it is grown as a crystalline thin film. For this reason is important to monitor levels of residual stress, inherited from such grown defects, and which can risk the mechanical stability of SiC- made thin film devices.

Stoney's equation is the theoretical foundation of the curvature method for measuring thin film residual stress. It connects residual film stress with substrate curvature through thin plates bending mechanics. Important assumptions and

simplifications are made about the film-substrate system material properties, dimensions and loading conditions; however, accuracy is reduced upon applying such simplifications. In recent studies of cubic SiC growth, certain Stoney's equation assumptions are violated in order to obtain approximate values of residual stress average. Furthermore, several studies have proposed to expand the scope of Stoney's equation utility; however, such expansions demand of more extensive substrate deflection measurements to be made, before and after film deposition.

The goal of this work is to improve the analysis of substrate deflection data, obtained by mechanical profilometry, which is a simple and inexpensive technique. Scatter in deflection data complicates the use of simple processes such as direct differentiation or polynomial fitting. One proposed method is total variation regularization of differentiation process; and results are promising for the adaptation of mechanical profilometry for complete measurement of all components of non-uniform substrate curvature.

Chapter 1.

Introduction

1.1 Motivation for research

Because of its favorable mechanical and electrical properties, silicon carbide (SiC) raised plenty of interest among fabricators of micro-electronic, optoelectronic, and micro-electromechanical thin film devices. SiC properties make this crystalline material preferable over currently used polysilicon for several electronic applications; these properties are wide band gap, and high breakdown electric field strength, high thermal conductivity, saturated drift velocity, elastic modulus and hardness. Moreover, SiC is extremely tolerant to harsh environment, which is constituted by abrasive and corrosive substances, extremely high operating temperatures, and low levels of friction [1, 2].

Commercial use of SiC for electronic devices began with substrate fabrication for blue and green light emitting diodes (LEDs); and actually, this has been one of very few successful commercial applications of SiC-based thin film devices. There is high interest, however, in research of SiC-based devices in a very wide variety of microscopic applications [2, 3]. In power applications with high voltage, SiC-based field effect transistors and power diodes have been developed with low on-state voltage drops and off-state leakage, and fast switching characteristics [4-6]. Additionally, SiC-based chemical field effect

transistors are being developed for gas sensing applications, such as exhaust monitoring in piston-cylinder, and turbine engines [7-9]. Lastly, another SiC application example lies in micro-electromechanical systems (MEMS) fabrication; and this presents an opportunity for SiC to outperform other materials; because its hardness, highest next to diamond; and tolerance of extreme operating conditions [10, 11].

SiC is a crystal that exists in more than 200 polytypes [12]. Each SiC polytype corresponds to a unique stacking sequence formed by the SiC unit; which can arrange itself in either a cubic, hexagonal, and rhombohedral form (such is the reason for polytype notation ‘C’, ‘H’ or ‘R’, and preceeding number corresponds to the number of layers involved in one sequence repetition). Hexagonal polytypes, 4H-SiC and 6H-SiC, have been widely used for bulk growth of substrates. Thin film growth of these two polytypes has also been achieved by the Chemical Vapor Deposition (CVD), mainly for microelectronic applications; however, homoepitaxial growth has only been possible on substrates of the same material.

Growth of SiC in both bulk and thin film forms is complicated and expensive; and thus it is currently non-feasible for device mass production. Because of the same properties that make SiC desirable, growth systems are required to meet very demanding thermodynamic conditions. Moreover, resultant defect density levels of SiC crystal structure are too high to control device failure, and efficiently grow substrates larger than 4 in [13, 14].

On the other hand, only cubic 3C-SiC can be epitaxially grown on a substrate of different material by CVD [15]. However, defect density is an ongoing issue of thin film quality; consequently, CVD process has been greatly improved over the last 2 decades, achieving significant reduction of defects, especially within layers above film-substrate interfaces. What makes CVD an appropriate deposition technique is repeatability, and versatility of film composition results [11, 16, 17].

Optimization of thin film quality is achieved by altering the CVD process; hence, there are various types of CVD reactors, which accomplish special conditions, such as lower chamber pressure, higher temperature, flow orientation of reactants, and plasma-enhanced reactions. Moreover, variable process parameters involve temperature and pressure in the reaction chamber, composition of reactants, substrate holder position, and substrate alignment. Consequently, each combination of variables generates a unique CVD process that achieves certain film qualities, e.g. thickness uniformity [18, 19]; epitaxial or amorphous growth [20-24]; film material purity [25-27]; and composition homogeneity [28, 29].

In the case of MEMS applications, 3C-SiC offers significant advantage over materials currently used (i.e. silicon among others); especially for applications that require operation within harsh environments [30]. Being a significant reason for developing 3C-SiC growth, film quality for MEMS application is characterized in terms of the film mechanical properties; which are hardness strength, and elastic properties [31].

The role of residual stress in thin films comes into play when studying mechanical integrity of thin films; it has a significant influence on film strength, and thus on device reliability. Additionally, high residual stresses can generate plastic deformation within material, and even promote inter diffusion of adjacent volumes of different compositions. For this reason characterization of 3C-SiC film quality involves an accurate understanding of resultant levels of residual stress.

Measurement of thin film residual stress can be performed by several methods, which vary in terms of what measured quantity, and theoretical approaches are related to residual film stress. Each measuring method includes a unique set of advantages, and challenges; consequently, appropriate technique selection must consider how much accuracy is affected by the interpretation of measured quantity, and the involved theoretical assumptions.

The present work explains how interpretation of measured quantity can be improved for a specific residual stress measurement technique, called the substrate curvature method, first proposed by Stoney for thin films deposited by electrolysis [32]. This technique is perhaps the most practical in terms of implementation; as it is non-destructive, inexpensive, and involves simple tool usage and post-measurement analysis. The following section will help the reader understand the mechanisms of formation of residual film stress, and how these affect its measurability. Next, and before presenting the work done with the curvature method, a brief review of residual stress measuring techniques will be given. Chapter 2 proposes a different approach for analyzing substrate

deformation, and Chapter 3 will provide conclusions and future recommendations.

1.2 Residual Stress in thin films

W.D. Nix presents a visual analogy to the sequence of events that is very helpful to understand the resultant physical loading in a film-substrate system; caused by the residual film stresses [33].

In this analogy, the substrate and films are represented as two thin plates; each having different lateral dimensions, and the film has a thickness much smaller than that of the substrate. Figure 1-a shows how both plates are initially un-strained. Then in Figure 1-b, film is uniformly strained among its volume by external forces located at the edges; causing the film lateral dimensions to match perfectly with those of the substrate (e.g. if the film originally has smaller width and length, then the external forces need to be of tensile nature). Next, film and substrate “adhere” to each other, so bonds hold both plates together, relieving the film from external forces. As a result, there is a “tendency” for the film to recover its original geometry. The film-substrate bonds are sheared at the edges of the plates; causing the substrate to deform into a new equilibrium state, as shown in Figure 1-c. The mentioned “tendency” is analogue to the causes of residual film stress.

There are several mechanisms that independently cause residual stress. These stress formation mechanisms are classified as thermal, epitaxial, or

intrinsic. First, thermal residual stress is generated due to the misfit in coefficients of thermal deformation, existing between film and substrate materials; moreover, film deformation is constrained by adhesion to the rigid substrate. Thermal stresses occur upon any temperature change; such as that experienced between film deposition event, and after-deposition exposure.

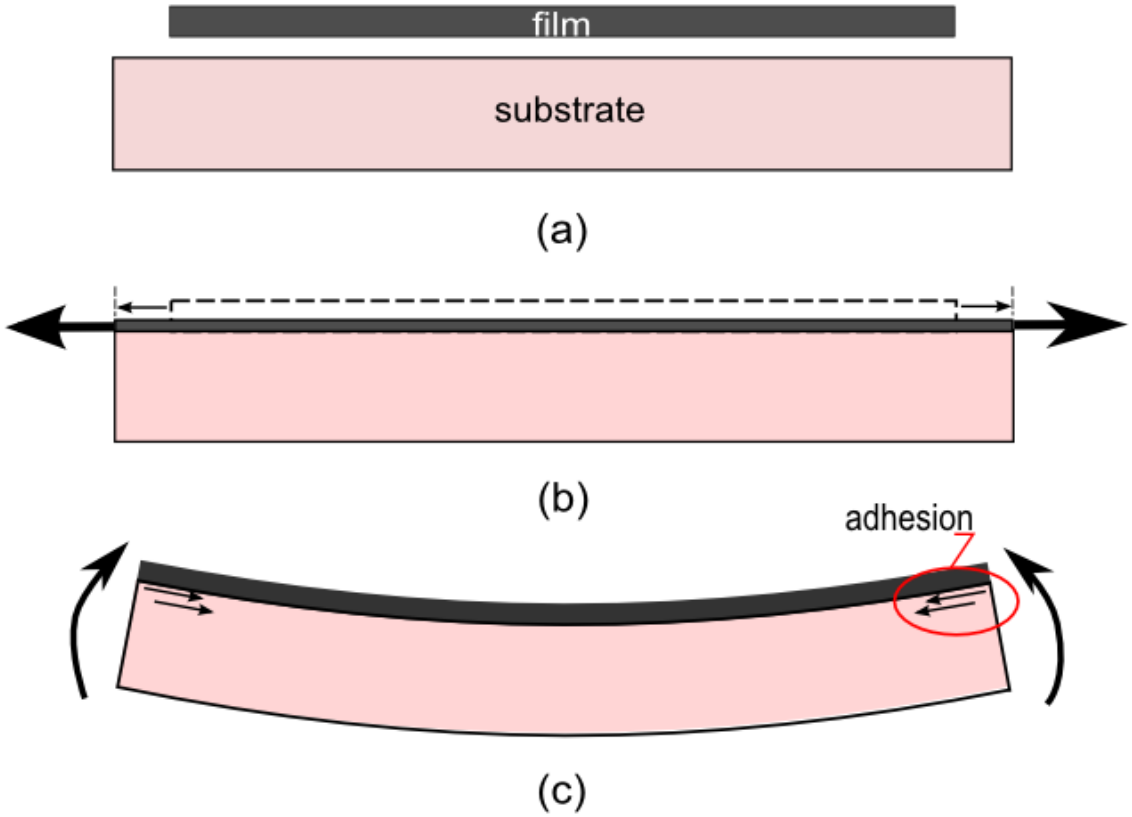

Figure 1. Sequential analogy to thin film deposition on substrate. a) Film and substrate are originally unstrained. b) External forces strain film to match substrate. c) Substrate and film achieve equilibrium state after deformation.

Epitaxial stresses are caused during epitaxial film growth, due to the misfit in crystal lattices existing between film and substrate (or underlying film) materials. Similarly, adhesion to rigid substrates prevents growing film from adapting to such lattice misfit, causing the mentioned epitaxial stress [33].

Lastly, intrinsic stresses are caused by volume changes that occur within the film material, and are induced by mechanisms of energy minimization. These mechanisms are related to epitaxial growth rate, atom mobility, point defects, impurities, granular growth, and phase transformations. As a consequence, stresses arise intrinsically upon any volume change, and due to the constraint imposed by the same structure of the solid film, and by adhesion between film and substrate [34].

In an actual film, epitaxial, thermal and intrinsic types of stresses are superimposed to a resultant residual stress, which can be large enough to generate significant deformations, or even failure of a thin film. In other words, stresses within film may translate in the form of substrate cracking; film delamination or buckling. Moreover, long-term presence of stresses within a film can promote diffusion-related processes within film-substrate system, such as densification of film material, and phase transformations. On the other hand, lower levels of residual film stress are equilibrated by film-substrate interactions [35-37].

Deposition parameters can control residual stress formation; however, because of the complexity and variety of mechanisms, studies are performed by focusing on specific combinations of materials and deposition technique. The CVD process parameters above-mentioned are also directed towards the controlling of resultant residual stress in a CVD film; clear examples can be seen in [38-44].

Evidently, it is important to understand what the mechanisms of residual film stress formation are; however, it is equally essential to understand at what length scale each stress source acts on. Intrinsic sources of stress keep the absolute residual film stress constant only over microscopic lengths; while effects of extrinsic and epitaxial stresses are macroscopically consistent, even throughout the entire film. In other words, the resultant residual stress made up by superimposed individual sources of stress, can be of a constant value over a certain volume of the film grown; or also, can vary even microscopically, and thus averaging to a certain value, or zero, over macroscopic volumes. For this reason, residual stresses are also classified into macroscopic and microscopic stresses. This classification is based on the length scale over which the value of an individual stress source makes up one period of oscillation within the thin film structure [45].

1.3 Curvature method for measuring residual stress

The main purpose of this work is to present a technique to measure residual film stress induced on a film after deposition. It was previously explained that the determination of stress over a certain volume significantly depends on the length scale; accordingly, different techniques vary in their resolution range [45]. Moreover, each currently available technique utilizes a certain theoretical approach which relates the residual stress in a film to a measureable property of

thin film-substrate system. The following paragraphs will briefly reveal the wide variety of residual stress measuring techniques that are currently used.

There are two measuring mechanism through which residual stress is frequently measured, one is by directly measuring strain, and the other by measuring bulk deflection of the film-substrate body. Strain-based techniques have many useful capabilities besides just measuring residual stress, such as identifying material elements and compositions, and analyzing crystalline structures [46].

The most significant theory of strain-based techniques is X-ray diffraction (XRD), from which many different instruments and measurement procedures branch out. This technology is based on Bragg's law, and its use is mainly intended for analyzing internal structure and composition of crystalline materials; nevertheless it has played a major role in the task of measuring residual film stresses [47]. Bragg diffraction allows for measuring spacing between crystallographic planes, which is unique for each specific crystal arrangement; this then permits for valuable identification and analysis of crystal type, structure, composition, and orientation. Additionally, material strain is quantified by measuring the change of inter-planar spacing that a film material undergoes after film deposition, with respect to its known un-strained spacing value. Subsequently, and under certain assumptions, stress and strain are related through elasticity theory (Hooke's law) [48, 49]

An extensive number of works has developed procedures based on XRD for measuring residual stress effects; each work intending to overcome a certain

challenge. For example, variation of strain with respect to film thickness has been determined through certain ways based on the $\sin^2\psi$ technique [50-53]. Glancing incidence XRD technique is used when small thicknesses only allow for small angles of diffraction [52, 53]. High resolution XRD has better capabilities for determining complete strain tensor information, and thickness profiles [54, 55]. In conclusion, XRD techniques can provide great detail of residual strain within materials at both microscopic inter-granular and intra-granular regions.

A limitation of Bragg diffraction techniques is that it only works for crystalline and polycrystalline materials. Anisotropy of materials is analyzed with XRD by measuring strain at the same surface location from various independent perspectives (directions). On the other hand, more complicated diffraction approaches have been proposed for amorphous structures [51, 56].

Raman spectroscopy is a different stress determination approach, which analyzes light spectra emitted by specific materials. A light beam, focused at a point-location of the film-substrate system, changes the internal energy of the compounds within the film material; and a specific light spectrum is obtained, specific to the material composition. The change of a certain peak can be related to the induced stress or strain. Implementation of Raman spectroscopy has been compared with other stress-measuring techniques, while characterizing SiC deposited by CVS [57-60].

The focus is switched now to techniques that measure deflection from a macroscopic perspective. These are developed from elasticity and mechanics of materials theories, relating the measured change of curvature in the substrate

plate due to bending loads caused by residual stresses. The most common, and also most simple theoretical relation between stress and substrate curvature change is Stoney's equation [32]. Its derivation will be explained in the following section, as well as how its idealistic assumptions deviate from actual film-substrate conditions. Popular stress measuring techniques that are based on this equation include optical interferometry [61-65], X-ray double crystal diffraction topography [66-69], optical profiling [69], and mechanical profiling [38, 70]. In summary, all techniques measure bending deflection of the substrate, caused by residual stresses. This work will make use of mechanical profilometry for the stress measurements.

Before comparing the above-mentioned techniques of stress measurement, it is useful to remember the importance of the length scale in stress measurements; explained in the previous section. Stress measurements taken at microscopic, or even higher scales, will determine the average stress value over that microscopic area, or volume; this is the case for XRD and Raman Spectroscopy instruments. Microscopic stresses may not be accurate indicators of the average stress across the film surface, or even across its thickness; however, they represent more precisely values of absolute stress [71]. On the other hand, macroscopic deflection-based techniques often make assumptions that imply an average stress value for the entire system, or at least for areas involving the entire thickness of the film; such measuring techniques do not bring microscopic stress variations into sight. Stress results from the curvature

(deflection) methods may present inaccuracies inside of an expected error range; but still are practical for average estimation of stress.

Instead of being an inconvenience, the aforementioned difference between microscopic strain-based techniques, such as XRD and Raman spectroscopy, and macroscopic deflection-based techniques, can instead be of complementary advantage. In other words, average stresses that are evaluated macroscopically can be compared with stress values that correspond to microscopically scaled regions. Conversely, different precision requirements can eliminate the use of a certain technique, or a certain instrument.

Macroscopic deflection-based methods have no restriction on the type of material subject of measurement, as opposed to XRD, by which amorphous materials cannot be analyzed. Moreover, such techniques have the capability of measuring stress variations along lateral dimensions. Instrumentation for curvature measurement is practical for an industrial environment, and also inexpensive, compared to XRD diffractometer.

1.4 Derivation of Stoney's equation

In order to set up the ground for Stoney's equation derivation; simplifications about the states of stress and strain of the thin film-substrate system are needed. First, thicknesses of such systems are small enough to be considered as thin plates. For the applications involved in this work, thin films correspond to an approximate thickness no larger than 200 μm; and substrates

to slightly over 500 μm thickness, and 50 mm diameter. Notice that film is significantly thinner, and it entirely covers the surface of a substrate. It is also assumed that both film and substrate materials are isotropic and homogeneous.

The film- substrate system is mainly under bending loads due to residual stresses present in the film. Effects from other loads types, including shear, can be neglected. Moreover, for the case of isotropic mechanical properties, the substrate should bend into a spherical shape, showing a uniform curvature across its surface. Lastly, substrate deflections caused by bending moment will be considerably smaller than any dimension of the substrate, even its thickness. Despite the fact that real internal loading of a film-substrate system is slightly more complex, these assumptions are the foundation of Stoney's equation.

A substrate is represented by a thin plate of uniform thickness. A plate is considered thin when its thickness is considerably smaller than its lateral dimensions. A Cartesian coordinate system shall be described such that *x* and *y* axes are horizontal, and parallel to the plate's surface; *z* axis is oriented along the thickness dimension. The origin is placed on the volumetric center of the plate. The *xy* plane located at z=0 is called the 'midsurface' of the plate, symmetrically dividing the plate's cross-section in two parts.

Given the small thickness of the plate, bending loads will cause negligible normal and shear strains parallel to the *z* axis. In other words, deformations from bending will not include any thickness change; and the plate's cross-section will remain perpendicular to the midsurface. These special conditions of deformation correspond to *plane strain* conditions, which define strain components as

$$\varepsilon_x = \frac{\partial u}{\partial x} \qquad \varepsilon_y = \frac{\partial v}{\partial y} \qquad \varepsilon_z = \frac{\partial w}{\partial z} = 0$$

$$\gamma_{xy} = \frac{\partial u}{\partial y} + \frac{\partial v}{\partial x} \qquad \gamma_{xz} = \frac{\partial u}{\partial z} + \frac{\partial w}{\partial x} = 0 \qquad \gamma_{yz} = \frac{\partial y}{\partial z} + \frac{\partial w}{\partial y} = 0 \qquad (1),$$

where ε_x, ε_y, ε_z are the components of normal strain oriented along x, y, and z coordinate axis respectively; γ_{xy}, γ_{xz}, γ_{yz} are components of shear strain parallel to their corresponding coordinate plane; and u, v and w are displacements of material along the x, y and z axes, respectively. Figure 2 shows an originally flat thin plate under bending, with the described coordinate system and plane strain conditions. The figure shows an exaggerated deflection w.

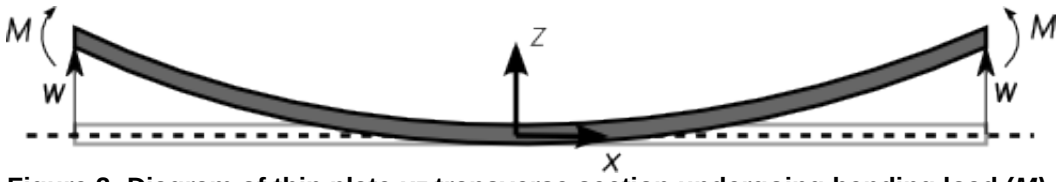

Figure 2. Diagram of thin plate *xz* transverse section undergoing bending load (*M*). Plate is bent concave upwards.

Knowing that ε_z equals zero implies that w is a function independent of z; thus it defines how the location of the midsurface varies from its original position, with respect to x and y coordinates. Pure bending conditions stipulate that the midsurface (any point at z=0) does not undergo strain.

For the case of a thin plate deformed concave upwards as shown above, material located on positive z axis will be under compression; while the opposite holds for negative z axis locations. Strain definitions described can be combined in order to derive that

$$\varepsilon_x = -\frac{\partial^2 w}{\partial x^2} z \qquad \varepsilon_y = -\frac{\partial^2 w}{\partial y^2} z \qquad \gamma_{xy} = -2\frac{\partial^2 w}{\partial x \partial y} z \tag{2},$$

where the negative signs explain the negative (compressive) strain at points on the positive z axis and vice versa.

Basic calculus helps explain that the curvature κ and radius of curvature r of a line $w(x)$ is

$$\kappa_x = \frac{1}{r_x} = \frac{\partial^2 w / \partial x^2}{\left[1 + \left(\partial w / \partial x\right)^2\right]^{3/2}} \tag{3},$$

where $w(x)$ is the line describing midsurface deflection, only as a function of x coordinate. For a specific location (x,y), certain radii of curvature r_x, r_y and r_{xy} exist; and they are parallel to xz, yz and xy planes, respectively. It was already noted that the applications of this work only involve small deflection values, such that the term $(\partial w / \partial x)^2$ is sufficiently small, and thus the equation above is simplified to

$$\kappa_x = \frac{1}{r_x} = \partial^2 w / \partial x^2$$

and similarly,

$$\kappa_y = \frac{1}{r_y} = \partial^2 w / \partial y^2 \qquad \kappa_{xy} = \frac{1}{r_{xy}} = \partial^2 w / \partial x\, dy \tag{4} .$$

Strains ε_x, ε_y and γ_{xy} within the thin plate can be expressed as functions of the corresponding location coordinates and curvature k; this is done by relating equations (2) with (4), obtaining

$$\varepsilon_x = -\kappa_x \cdot z \qquad \varepsilon_y = -\kappa_y \cdot z \qquad \gamma_{xy} = -2\kappa_{xy} \cdot z \qquad (5)\ .$$

It will be shown that this relation is very useful for the physical determination of intrinsic stress. By using Hooke's law and equation (5), stress of a plate element will be related with its curvature. Based on the fact that substrate thickness and bending deflections are significantly small, stress component σ_z is neglected. Hence the stress state within any location of the plate will be described by

$$\sigma_x = \frac{E}{1-\nu^2}\cdot\left(\varepsilon_x + \nu\varepsilon_y\right) = \frac{E}{1-\nu^2}\left(\frac{\partial^2 w}{\partial x^2} + \nu\frac{\partial^2 w}{\partial y^2}\right) = -\frac{E\cdot z}{1-\nu^2}\cdot\left(\kappa_x + \nu\cdot\kappa_y\right)$$

$$\sigma_x = \frac{E}{1-\nu^2}\cdot\left(\varepsilon_y + \nu\varepsilon_x\right) = \frac{E}{1-\nu^2}\left(\frac{\partial^2 w}{\partial y^2} + \nu\frac{\partial^2 w}{\partial x^2}\right) = -\frac{E\cdot z}{1-\nu^2}\left(\kappa_y + \nu\cdot\kappa_x\right)$$

$$\tau_{xy} = \frac{E}{2(1+\nu)}\cdot\gamma_{xy} = -\frac{E\cdot z}{2(1+\nu)}\cdot\frac{\partial^2 w}{\partial x\partial y} = -\frac{E\cdot z}{2(1+\nu)}\cdot\kappa_{xy} \qquad (6),$$

where σ_x and σ_y are the functions of normal stress along x and y axis respectively; τ_{xy} is the shear stress, parallel to the xy plane. E and ν are the Elastic Young's modulus, and Poisson's ratio, respectively.

Like in any loading case of pure bending, each component of stress is distributed linearly, along the orientation perpendicular to the stress action. The

'neutral surface' is that on which normal stress equals zero, as seen in equation (6); and because of symmetry properties, such surface coincides with the midsurface (i.e. any point at which z=0). This is connected with the fact noted in equation (5), which results in zero strain at the mentioned surface $z=0$. As the location z varies towards the top and bottom plate surfaces, each stress component increases linearly, also depends on the corresponding curvature $\kappa=1/r$, and on a constant $E/(1+\nu)$, which is called the 'biaxial elastic modulus' of an isotropic material. Figure 3 shows a two-dimensional diagram of the stress profile along a cross-section of the plate parallel to the xz plane. Note that profiles are identical for a section in the yz plane.

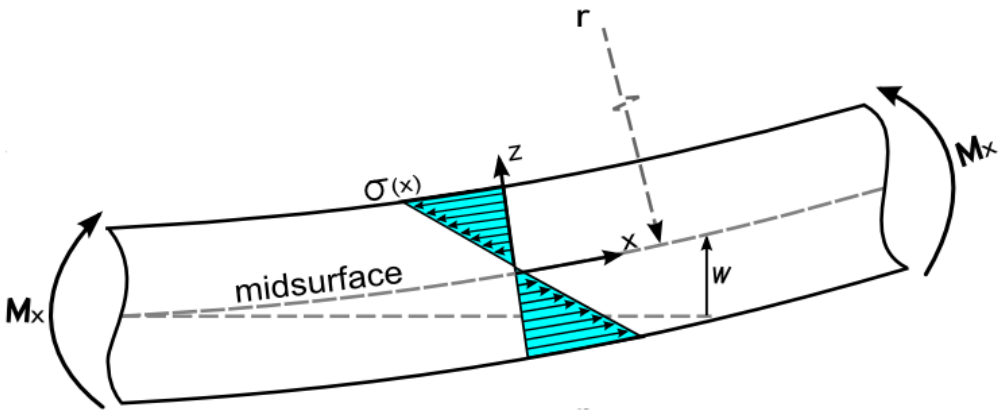

Figure 3. Transverse section in *xz* plane of a thin plate with a normal stress σ_x profile caused by bending moment M_x.

Figure 3 shows that stress distribution is symmetrical; hence it corresponds to zero net force, and to a certain bending moment component M_x.

Accordingly, each stress distribution σ_x, σ_y and τ_{xy} is related to bending moment components M_x, M_y, or M_{xy} respectively. These stress-moment relations are

$$M_x = \int_{-t/2}^{t/2} z \cdot \sigma_x \, dz \qquad M_y = \int_{-t/2}^{t/2} z \cdot \sigma_y \, dz \qquad M_{xy} = \int_{-t/2}^{t/2} z \cdot \tau_{xy} \, dz \tag{7},$$

where t is the plate thickness, and the integral is evaluated over the entire transverse section, along the z axis, and with integration boundaries from $z=-t/2$ and $z=t/2$. If equations (6) are combined with (7), local moment components are related to the midsurface curvatures, resulting in

$$\begin{aligned} M_x &= -D \cdot \left(\frac{\partial^2 w}{\partial x^2} + \nu \frac{\partial^2 w}{\partial y^2} \right) &&= -D \cdot \left(\kappa_x + \nu \cdot \kappa_y \right) \\ M_y &= -D \cdot \left(\frac{\partial^2 w}{\partial y^2} + \nu \frac{\partial^2 w}{\partial x^2} \right) &&= -D \cdot \left(\kappa_y + \nu \cdot \kappa_x \right) \\ M_{xy} &= -D \cdot (1-\nu) \cdot \frac{\partial^2 w}{\partial x \partial y} &&= -D \cdot (1-\nu) \cdot \kappa_{xy} \end{aligned} \tag{8},$$

where $D = \dfrac{E \cdot t^3}{12 \cdot (1-\nu^2)}$.

Due to the fact that the film is much thinner than the substrate, the film stress is interpreted as a point load on the top edge of the substrate. A force and a moment are reaction loads located at the center of the substrate section; and have the purpose of equilibrating the film stress.

Figure 4 shows the loaded film substrate system with the corresponding internal stresses. Below, equilibrium equations for the loads and moments are

$$\sum F: \quad \sigma_f t_f - \sigma_s t_s = 0 \tag{9},$$

$$\sum M: \quad \sigma_f \cdot t_f \cdot \left(\frac{t_s}{2}\right) + M_x = 0 \tag{10},$$

where the subscripts s and f indicate substrate and film, respectively; t is the thickness, as shown on Figure 4.

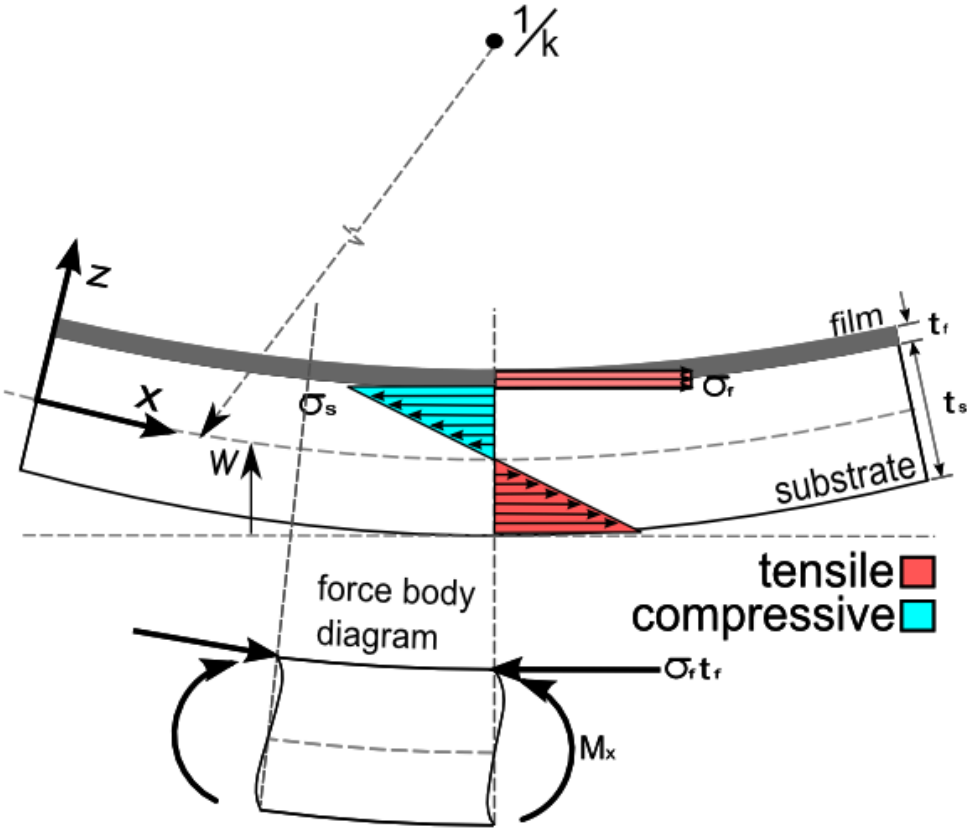

Figure 4. State of stress and loads of a thin film – substrate system.

The moment M_x is described in equation (8), with the subscript 'x' noting that it corresponds to the stress component σ_x; however, this moment acts about the y-axis. Equations (8) and (10) are combined to describe film stresses in terms of substrate curvatures:

$$\sigma_{x,f} = \frac{E \cdot t_s^{\,2}}{6 \cdot (1-\upsilon)^2 \cdot t_f} \cdot \left(\kappa_x + \upsilon \cdot \kappa_y\right)$$

$$\sigma_{y,f} = \frac{E \cdot t_s^{\,2}}{6 \cdot (1-\upsilon)^2 \cdot t_f} \cdot \left(\kappa_y + \upsilon \cdot \kappa_x\right)$$

$$\tau_{xy,f} = \frac{E \cdot t_s^{\,2}}{6 \cdot (1-\upsilon)^2 \cdot t_f} \cdot \kappa_{xy} \qquad (11),$$

where $\sigma_{x,f}$, $\sigma_{y,f}$ and $\tau_{xy,f}$ are the corresponding intrinsic film stresses in the respective directions.; in the other hand, material properties E and v correspond to those of substrate.

Finally, thicknesses of both film and substrate are assumed to be uniform in any direction of the whole system. Misfit strain existing in film is similarly uniform. For this reason, shear stress would not be present at the film-substrate interface. Additionally, curvatures and stresses along any orthogonal set of directions are equal; or in other words, curvature and stresses are equibiaxial. These important simplifications have allowed Stoney in [32] to generate this famous relation, which summarizes the stress of thin film as a single value:

$$\sigma_f = \frac{E \cdot t_s^{\,2} \cdot \kappa}{6 \cdot (1-\upsilon)^2 \cdot t_f} \qquad (12)$$

where $\sigma_f = \sigma_{x,f} = \sigma_{y,f}$, and $\kappa = \kappa_x = \kappa_y$. Next chapter will explain how κ is calculated, by first indicating that for initially deflected substrates, residual film stress σ_f from equation (12) is actually dependent of the change of substrate curvature, which occurs after deposition process, and such change is noted as $\Delta\kappa$.

1.5 Limitations and modifications of Stoney's equation

Stoney's equation is based on simplifying assumptions about the properties, and conditions of film-substrate system; allowing for this relation to be extensively used for the estimation of residual film stress. There is no need for prior knowledge of substrate properties; and simple measurement techniques are required. These assumptions were previously described, and are now summarized:

1. Substrate and film are represented by a thin plate and a membrane, respectively; or, $t_f << t_s$.
2. Substrate bending deflections are small compared to any dimension.
3. Film and substrate material properties are homogeneous, isotropic or in-plane symmetric and linear elastic.
4. Film stress is in-plane isotropic, or equibiaxial. Shear stresses and out-of-plane stress components are negligible.
5. Substrate curvature change is uniform and equibiaxial. Twist curvature component is negligible.
6. All stress and curvature components remain constant across entire wafer.

A similar summary list can be read elsewhere [72]. These assumptions imply several limitations to the applicability of Stoney's equation; and for this reason, actual film-substrate system conditions often deviate from such idealizations. However, Stoney's equation has drawn enough interest, even for

its misuse, on film substrate conditions that violate the implied limitations; hence, errors in results are inherited. Often, the purpose of studies allows for less accuracy, thus Stoney's equation results are then accompanied with a logical margin of error, and appropriate validation.

Assumption #1 may yield inaccuracies on cases when thickness of film is not constant over the entire surface. CVD thin films might become an example when gas reactants incidence is not uniform over the substrate surface; in addition, patterned films are also clear examples of film thickness non-uniformity. Variations in film thickness generate non-uniform substrate curvature, and film residual stress distributions across the entire film. Solutions for these cases have been derived and recently proposed for several cases [72].

(100) oriented crystals, such as SiC and Si, are in-plane isotropic; for this reason, are not well described by the biaxial modulus *E/(1-v)* of equation (12); as a result, assumption #3 shall be relaxed by applying a modified version of this equation; which for a (100) oriented crystal, has already been derived; namely,

$$\sigma_f = \frac{t_s^{\,2} \cdot k}{6 \cdot (s_{11} + s_{12}) \cdot t_f} \qquad (13),$$

where $1/(s_{11} + s_{12})$ is the (100) crystal biaxial modulus; s_{11} and s_{12} are two of the three independent components of the material compliance matrix [33]. Previous validation works have confirmed on the accuracy of such modifications of Stoney's equation; however, uniformity of stress and curvature remains valid for each in plane orientation of film and substrate [73-76].

In the case of very high residual stresses, or when substrate is sufficiently flexible, large substrate deflections can become non-linear. In this case, assumption #2 is no longer valid; substrate deformation becomes non-axisymmetric, violating assumption #4. Solutions for these cases have been described several possible equilibrium states of a film-substrate system [77-80]. Past works have also concluded on a film stress threshold below which Stoney's equation remains valid. Above this "critical stress" level, non-linear deformations occur, obtaining shapes other than spherical, such as cylindrical, or ellipsoidal, which achieve a lower energy state. These shapes would then be described by biaxial, or even non-axisymmetric curvature, and stress components [81, 82].

Another example of Stoney's equation extensions is proposed for non-axisymmetric substrate deflection when radius of curvature is measured along two orthogonal orientations, R_1 and R_2, respectively [83]. In this work, modified Stoney's equation would look like

$$\sigma_f = \frac{E_s}{1-\nu_s} \cdot \frac{{t_s}^2}{6 \cdot t_f \cdot R_1} \cdot \left[1 + \left[\frac{\nu}{1-\nu} \right] \cdot \left[\frac{R_1}{R_2} - 1 \right] \right] \quad (14).$$

Finally, film stress, and substrate curvature can be non-uniform for many reasons; resulting in the non-validity of assumption #6. Reasons for this include non-uniform misfit (thermal or epitaxial) between material properties of films and substrate, structural defects, and non-uniform stress relaxation. This has been the most complicated case for numerical analysis to solve.

Typically, such realistic issues have been “set aside”, by simply measuring substrate curvature, either as average values through simple optics; or via profilometry, as functions of horizontal position x, $\Delta k(x)$ and $t_f(x)$ respectively. These curvature and thickness profiles (or functions of x) could be “inserted” into equation (12) for obtaining function $\sigma(x)$; yielding a residual stress profile, which is assumed to be axisymmetric, and vary across the substrate surface. The fact of substrate curvature change being non-uniform along a certain direction is enough evidence that non-uniform shear stress components existed in the film-substrate interface; and consequently, equilibrium equation (10) would not be valid. Nevertheless, this localized approach has been consciously taken by validating results, e.g. by using finite element modeling; and propose an acceptable margin of error [38].

Extensive work has been done in this matter by some of the authors already referenced in this section. Non-uniform stress and curvature components are derived from several driving conditions, such as non-uniform temperature distributions, arbitrary film thickness, and non-uniform misfit strain. Conclusions have been consistent, indicating that local residual stress values depend on local and even non-local curvature information, about the entire substrate. For this reason, the authors have suggested the need for measuring curvature components over the substrate, in order to obtain a full field profile of residual stress [72, 84-88].

Several techniques have been proposed to determine curvature across entire surface; however, they require more expensive tools than mechanical

profilometry [71]. This work would serve as an aid to develop an appropriate procedure of full field deflection measurement via mechanical profilometry.

Chapter 2.

Analysis of Substrate Curvature

2.1 Substrate deflection measurements

Equation (4) requires measure of substrate deflection w in order to use; and determine substrate curvature κ, induced by residual film stress. Previous section explained that under thin film assumptions, w describes how the substrate deflects in the z direction. Both w and κ are functions of the horizontal position x of a round substrate. Equation (4) was based on the assumption that deflection w is sufficiently small, such that the term $\left[1+\left(\partial w/\partial x\right)^2\right]^{3/2}$ could be neglected. Otherwise, the more complicated equation (3) would be required.

Blank substrates are almost flat when manufactured; nevertheless, small initial substrate curvature should be subtracted from the after-deposition curvature. Accordingly, equation (4) would then look like

$$\kappa = \frac{\partial^2}{\partial x^2}[w_2] - \frac{\partial^2}{\partial x^2}[w_1] \qquad (15),$$

where w_1 and w_2 are the measured substrate deflections before and after deposition process, respectively. Curvature κ is now more appropriately called ‘curvature change’.

The thin plate approximation allows for the surface height of a substrate to be a direct measure of the midsurface deflection w, from the original plane at z=0. Surface profiling was performed with the a Tencor P-20 Profilometer, which uses a mechanical stylus that measures with a vertical (height) resolution of 10 Å. Profiles were measured along lines collinear with the center point of circular substrates. Figure 5 shows scan lines of different orientations in which profiles could be scanned. A coordinate system was defined with its origin located at the start point of every scan; in other words, $w(0)$=0. In the case of films deposited by CVD, the opposite edge with respect to the silicon wafer flat is the x=0 point, with positive x axis oriented towards the flat edge. Reactants first arrive at this point; then follow a path along the 0° line, towards the opposite edge. All future plots that describe profiles of substrate deflections, and curvature, will utilize this coordinate system. Furthermore, scans will be centered about the wafer center, meaning that the middle point in the plotted x axis will correspond to the wafer center.

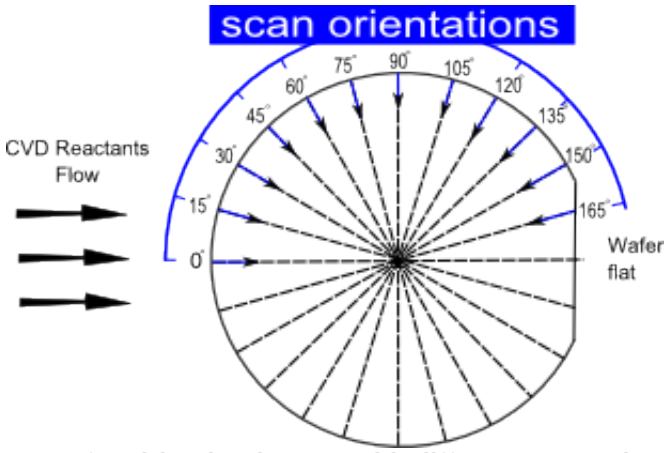

Figure 5. Diagram of a Si (100) substrate with different scan orientation angles.

3C-SiC films were deposited by CVD on 2 inch-diameter Si(100) substrates. Deflection measurements were performed at selected orientations, in order to account for non-uniformities that, as opposed Stoney's assumptions, may arise from material anisotropy; and non-uniform film thickness, material composition, and misfit strain. Furthermore, prior knowledge of the specific CVD reactor indicated that film thickness would follow variation in the form of linear, and parabolic profiles, along the 0°, and 90° directions, respectively [89]. Non-uniform film thickness could significantly limit the validity of Stoney's assumptions regarding uniformity and axis-symmetry. For this reason, thickness measurements of deposited 3C-SiC films were performed by FTIR spectrometry, along the 0° and 90° orientations [38]. Example of film thickness data is shown, and curve-fitted in Figure 6.

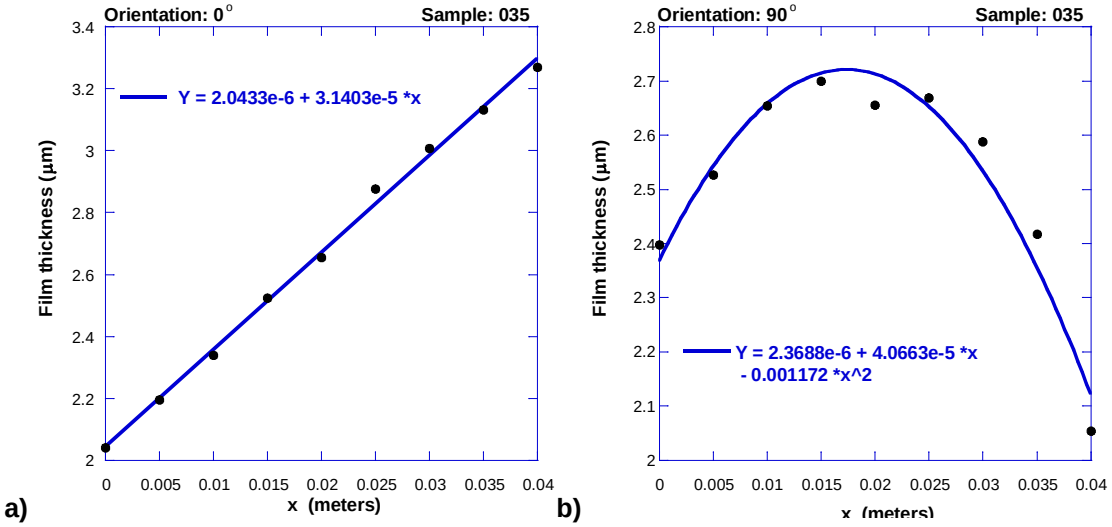

Figure 6. Thickness of CVD deposited 3C-SiC films along two orthogonal orientations. Measurements are a) parallel, and b) perpendicular, with respect to flow of gases.

Following equation (15), before, and after- deposition measurements of deflection were performed, and plotted as shown in Figure 7. Next, data from

previous experiments was added to the analysis of curvature for comparison purposes, as thickness non-uniformities in CVD grown SiC films present a challenge for analysis. Previous study [70] involved magnetron-sputtered tungsten thin films on 100 mm-diameter Si substrates. Besides W film thickness not being constant, it had axis-symmetric profile variations.

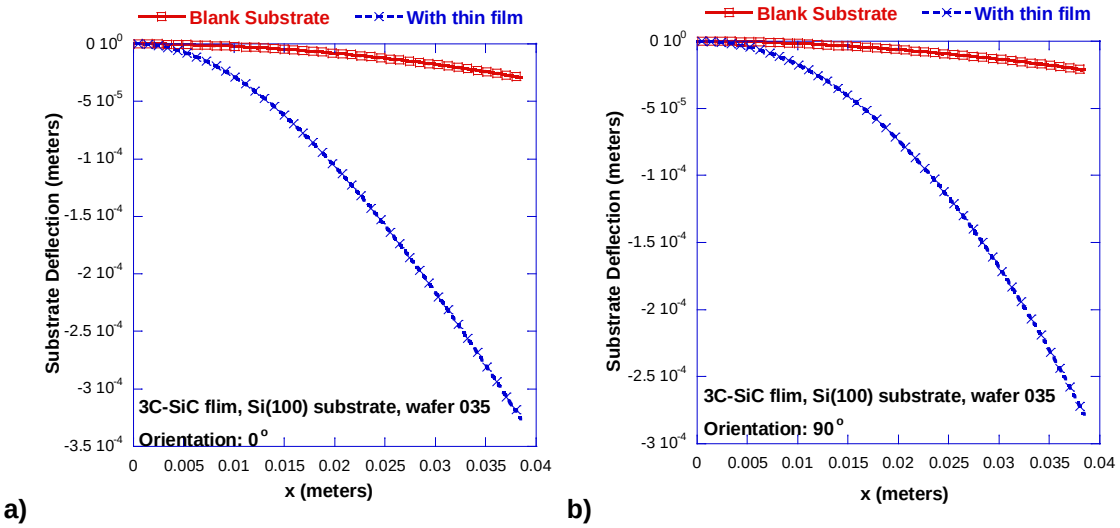

Figure 7. Substrate deflection data for 3C-SiC films along two orthogonal orientations. Measurements are in a) parallel and b) perpendicular orientations with respect to gases flow.

2.2 Data analysis by polynomial curve fitting

Polynomial regression was used to fit deflection data of each blank substrate; before and after deposition. Thus, functions describing substrate deflections along each measured orientation were obtained. Each function was then differentiated twice with respect to x for determining the terms on the right

side of equation (15). Finally, induced curvature change for each direction was obtained. Curvature change functions evaluated over the same domain of original data are plotted in Figure 8. This figure is also a clear indication that blank Si substrates were indeed close to being flat, prior to film deposition.

The polynomials used for curve fitting were first selected to be of 3rd order. The same procedure was then repeated for implementing each polynomial degree between 3 and 10; hence, 8 different functions were obtained to represent the substrate curvature of each sample-orientation combination. Curvature change results for 3C-SiC films on Si substrates are shown in Appendix A. Moreover, variation among different fits of the same data set was quantified for analyzing consistency between fits, and for comparing with results from a another analysis method, which is based on regularization of data (presented in the next section).

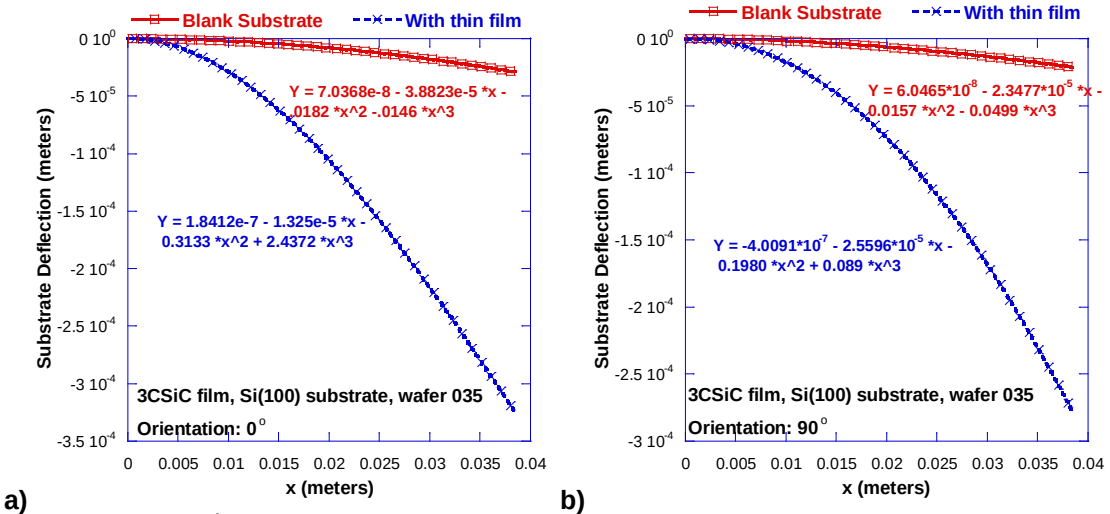

Figure 8. 3rd order polynomial fitting of substrate deflection for a) 0°and b) 90° orientations, and c-d) their second derivatives, respectively.

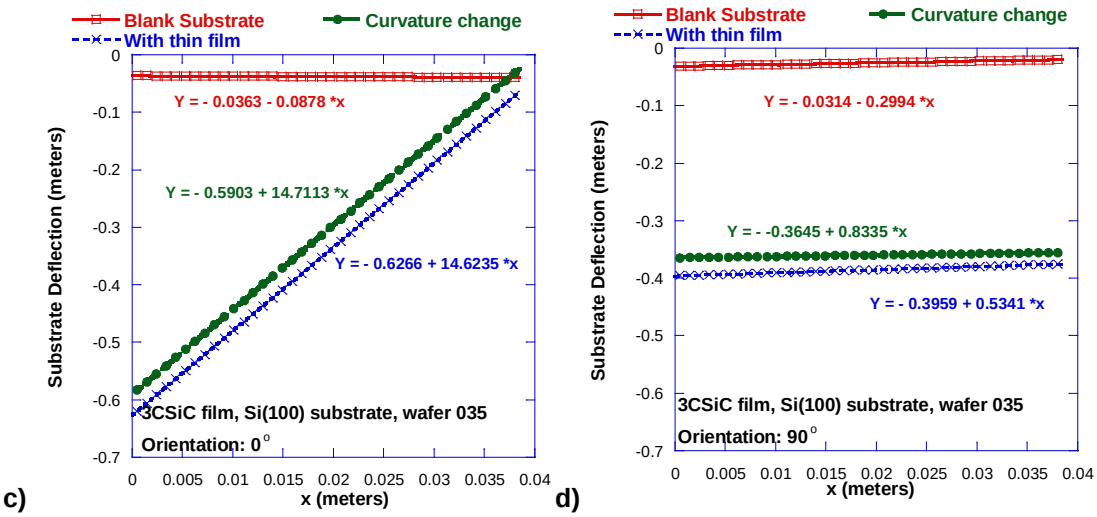

Figure 8. (Continued)

Average with standard deviation of substrate curvature was extracted at every interval of the *x* axis, from all profiles of different degree polynomials. Plots shown below would indicate how average curvature change results vary with respect to *x*, as well as how variation from this average is dependent of location along the substrate diameter. Regardless of the not-random nature of this variation, standard deviation was found useful for indicating inconsistencies between different fits.

For the case of 3C-SiC films, all Si substrates concaved downwards upon film deposition; corresponding to negative values of curvature change, and compressive stress (see equation (12)).

Figure 9 shows an example of average curvature change in a 3C-SiC films on Si wafer, along 0° and 90° orientations. Along CVD gases flow (0°) direction, amount of substrate curvature change varied in a decreasing manner; starting between -0.3 m^{-1} and -0.5 m^{-1} at the *x=0* edge, and ending between 0 m^{-1} and 0.2

m^{-1} at the *x≈0.04 m*. Oppositely, along the 90° direction, there was a more constant change-of-curvature trend, varying no more than 0.5 m^{-1} over most of substrate scan lengths.

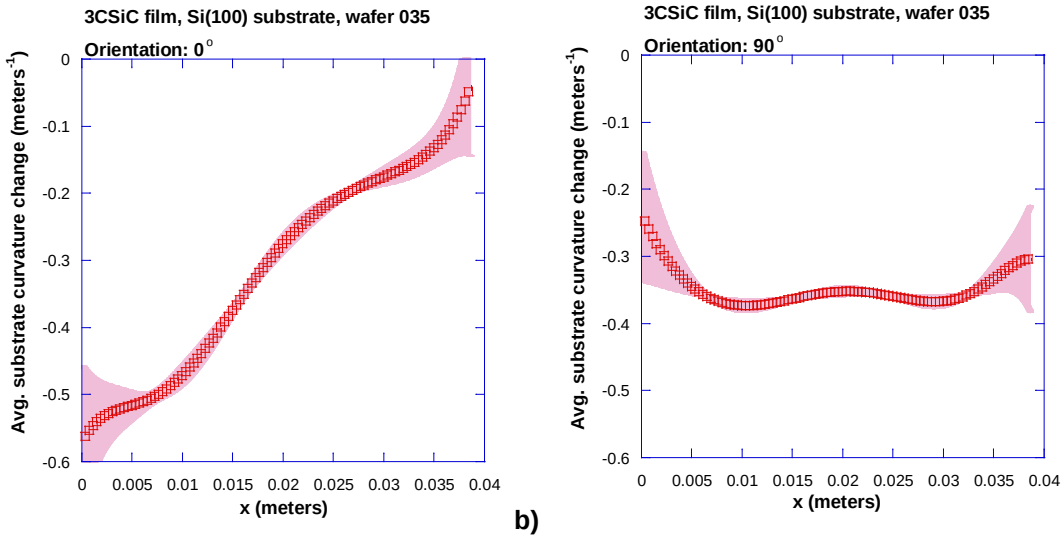

Figure 9. Average polynomial describing curvature change of 3C-SiC on Si (100) systems. Average profiles are derived from all polynomial fits along a) 0° and b) 90° orientations.

Plots from Appendix A, and Figure 9 also show the corresponding variation from the average substrate curvature profile, represented by the shaded region. There was significant variation of curvature change values along the 5 mm edge of the substrate. Without additional information, correct curvature values at the substrate edges are unknown.

Analysis from the W films on Si substrates was also performed for comparison purposes; resultant curvature change plots are shown in Appendix B. For this sample, there was data on 12 wafer orientations available (all angles of measurement are shown back in Figure 5). Substrate curvature change resulted negative across the entire length of all scans (compressive residual stress). A maximum of -0.03 m^{-1} curvature change (approximately) in the substrate center;

and minimum less than -0.01 m^{-1}, at the edge regions, were determined. Furthermore, consistency along 12 wafer orientations from 0° to 165°, in steps of 15°, indicated axis-symmetry of wafer curvature change. Significant variations are found at the edges of substrates and also, in the middle. Figure 10 shows 2, of the 12 orientations considered for curvature analysis.

The sole behavior of polynomials used for curve fitting can induce significant error upon calculation of second derivative. In general, fitting functions are constrained to describe all data points. However, polynomial behavior outside of the data domain is unique to their corresponding degrees, and the coefficient of its leading function term. When the polynomial degree is sufficiently high, degrees of freedom increase at the ends of data domain. By degrees of freedom, it is meant that the rate of change of the describing function is not entirely defined by the data, but by the sole nature of the specific polynomial.

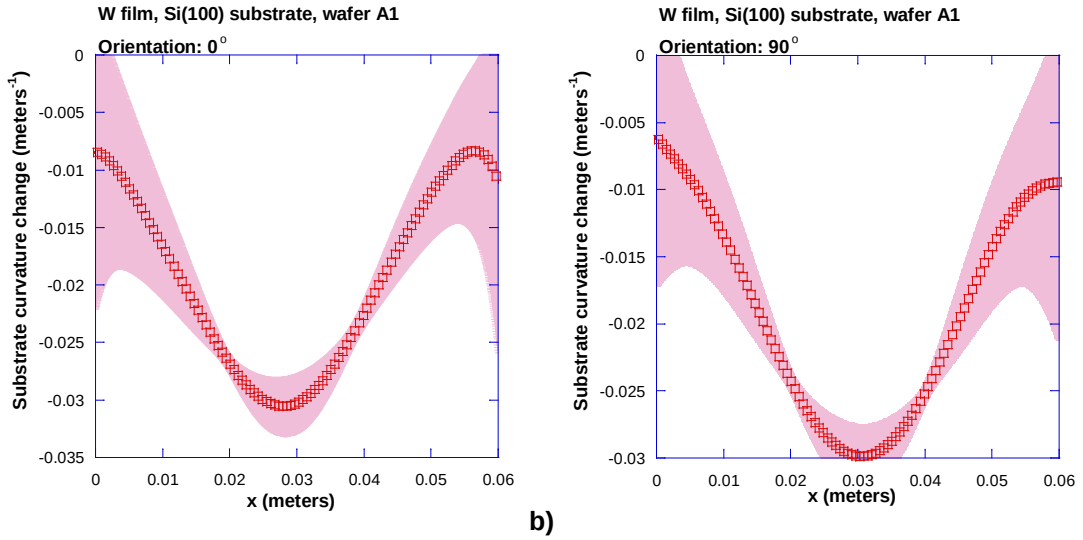

a) b)

Figure 10. Average polynomial describing curvature change of W on Si (100) systems. Average profiles are derived from all polynomial fits along a) 0° and b) 90° orientations.

Next, when looking at the second derivatives, these uncontrollable rates of change are represented by abrupt spikes, or sudden peaks. The slope of a curvature-change vs. x plot in these edge regions depends of the sign of the function leading term coefficient; and also, if the polynomial degree is an even, or an odd number. This explains the existing variation of curvature change values at the edges of the substrate.

Another source of error arises, when low enough polynomial order limits the possible number of local maxima, minima and inflection points that a fit can use to describe data. For this reason, a certain fit would not adapt well to a large presence of sharp curvature changes. Smoothness is always forced upon curvature profile, regardless of the polynomial order; hence, discontinuities created by surface scratches, may not be traced. Local stress fields may have been disregarded because of such inaccuracies.

A great inconvenience is that the above-mentioned sources of error can all be present in a single curve fit. Moreover, an appropriate fit is impossible due to lack of knowledge of additional information about true substrate deflection. On the other hand, the locations of significant variations are an indication that real substrate curvature is unrecognizable by polynomial fitting alone.

2.3 Segmentation of substrate deflection data

Polynomials are not adequate for analyzing 2^{nd} derivative of substrate deflection data; consequently, a different approach is taken for data curve-fitting.

It has been explained how a single polynomial fit can possibly over-estimate substrate deflection, when excess degrees of freedom could lead to sharp curvature changes, when actual substrate curvature had been constant over corresponding length segment. Simultaneously, on different length segments of the same data set, the same polynomial fit might not trace abrupt changes of real substrate curvature, because of the flexibility constraint imposed by its order.

A different approach for data curve fitting is to generate different fits on every equally divided segment of a single data set. First, substrate deflection data was equally divided into a certain number of segments; next, each segment was fitted with a second order polynomial. As a result, the second derivative of each fit would then yield a constant curvature for each segment. Consecutive segments would be represented by margins that have coinciding boundaries; hence, it is assumed that real substrate curvature at the edge of segments match with the margins. Continuity is implied as long as substrate does not have or discontinuities from cracking, film delaminating, buckling, or other forms of failure.

A probable advantage of applying data segmentation is that different surface features, such as sharp curvature changes, and constant flat sections, could be analyzed independently. However, length of data segments should be kept large enough to avoid deceptive influence from data scatter, and small enough to offer flexibility to changes in substrate profile.

Simulated data was generated in order to optimize the number of segments used in the above-described method of substrate deflection analysis.

Simulation of substrate deflection measurement was from a polynomial fit of real substrate deflection data, and added Gaussian noise with certain signal-to-noise ratio (SNR), which simulates data scatter. Several models were created with different polynomials, and SNR values; these are described below. Second derivatives of simulated deflection profiles were then extracted to compare with results provided by segmentation method.

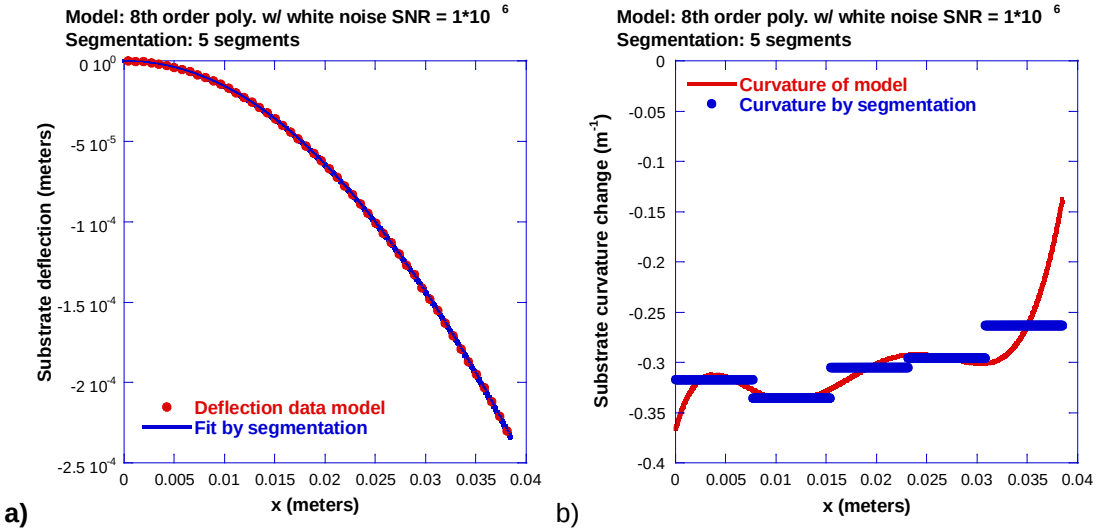

a) b)

Figure 11. Segmentation method applied to deflection data simulation. a) Segmented fits of deflection data. b) Segmented substrate curvature change.

Optimization was done by selecting the number of segments that generates least average residual between resultant curvature profile from segmentation method, and real curvature profile of each data model. Figure 11(a) shows segmented substrate deflection profile using “5” segments; and Figure 11(b) shows profiles of segmented substrate curvature, real (and continuous) substrate curvature of one data model. The squared norm of resultant residual between segmented curvature, and real curvature profiles was

the main criteria utilized to judge how accurate results are when using a certain amount of segments.

Figure 12 shows all resultant residuals generated by using each possible number of segments from 1 to 45, and each data model used. When using 10 segments, close to minimum residual is obtained, and resultant curvature segments follow the real curvature profiles well. For this reason, division by 10 segments was applied to all substrate deflection data. Results are also shown in Appendix A for 3C-SiC films on Si (100) substrates, and on Appendix B for W films on Si (100) substrates.

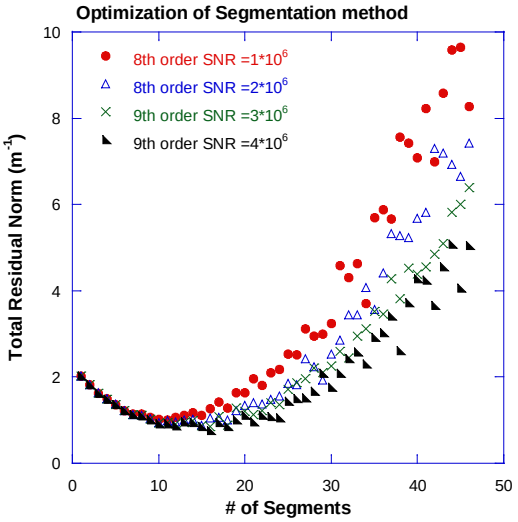

Figure 12. Optimization of segmentation method by selecting number of segments that yields lower residual norm for all substrate deflection models used.

2.4 Regularization method

The problem of determining the second derivative of a discrete data set, which has certain degree of scatter, constitutes an ill-posed problem [90].

Presence of small scatter amplitude is enough for magnifying error when differentiation of data is conventionally applied; especially double differentiation. FFT filtering can cause significant loss of information, which would otherwise indicate local film stress fields. Additionally, FFT does not sufficiently eliminate noise magnification [91, 92].

Studies in the field of image reconstruction and surface analysis have overcome this type of ill-posed problems through a process called Tikhonov Regularization [93]. A regularized signal is that which has a reduced amount of scatter, variation, or other form of irregularities expected to signify error. Instead of directly applying this process to a measured signal, or data set; past works have implemented it to regularize the process of differentiation itself, and thus calculated a regularized derivative of a discrete signal, while concurrently avoiding propagation of error [94].

The way that regularization of the differentiation process works is by minimizing the function *R,*

$$R(u) = \alpha \cdot A(u) + B\big(I(u) - f\big) \tag{16},$$

where *A* represents the size of noise, or scatter, that is to be regularized from the desired solution *u*, which is the derivative of the original signal *f*. This first term is scaled by a pre-selected regularization parameter α. *B* quantifies the difference between *f*, and the discrete integration of *u*, determined by trapezoidal rule and evaluated over the entire domain of *f*, at regular intervals *Δx*. A certain

computation method is required to determine an optimum form of *u* that minimizes *R*.

Regularization parameter provides the correct balance between amount of regularization applied to the signal, and the accuracy that is sacrificed. Appropriate selection of this value is not a straight forward procedure, and it depends on the relative amount of signal irregularity with respect to the expected true signal behavior. Without an elaborate numerical approach, trial and error can be enough to find an appropriate parameter value; however, some prior knowledge about what should the solution be, is required.

The way that *A* and *B*, from equation (16) are defined depends on the type of regularization used; and each provides a different effect on the solution. Tikhonov regularization utilizes the Euclidan, or L^2 norm for defining functions *A* and *B*. The effect of this type of regularization is that it forces smoothness upon *u*. On the other hand, a slightly different method called Total Variation Regularization (TVR) is able to recognize non-continuities in the solution [95].

Total variation is the absolute amount of vertical distance that any function *g(x)* covers in a *g* vs. *x* plot, determined through the L^1 norm of *g'*, namely,

$$. \; TV_{g(x)} = \int_0^L \left| g' \right| \cdot dx \qquad \textbf{(17),}$$

Furthermore, Chartrand combined TVR with the objective of regularized differentiation into a regularization algorithm utilizing the gradient descent method for minimization purposes. This algorithm was proposed as a tool for determining

first derivative of noisy, non-smooth, one-dimensional signals [96]. Accordingly, *R* is modified as

$$R(u) = \alpha \cdot \int_0^L | u' | + \frac{1}{2} \int_0^L | I(u) - f |^2 \cdot \quad \textbf{(18),}$$

where the data domain is defined from *x=0* to *x=L*; and the terms *A* and *B* in equation (18) are respectively defined by the L^1 norm of derivative solution *u*, and L^2 norm of the differential term described in equation (17). The gradient descent method was utilized by the algorithm author, Chartrand, in order to minimize equation (18).

In this work, substrate deflection data was differentiated through total variation regularized differentiation (TVRD), explained above; however, the original algorithm (provided by the abovementioned author) was modified for making *u* be the second, instead of the first derivative of *f*. Modification involved the substitution of *I* to be defined as a double integral over the same domain. As a result, curvature profile of deflection data was obtained. Integration constants were handled implicitly by prior translation, and rotation of data, so that *w(0)=0*; and that $dw/dx\big|_{x=0} = 0$. Appendix C of this work shows the minimization algorithm as written in Matlab syntax.

A range of possible regularization parameters *α* was selected by an evaluation process of TVDR results, using simulation of actual substrate deflection measurements. Simulation was based on several deflection data

models, which were generated by polynomial fits of real substrate deflection data, and Gaussian noise was added with an appropriate signal-to-noise-ratio (SNR), so that scatter from real measurements is well simulated. Second derivatives of simulated deflection profiles were extracted for the purpose of validating TVDR results from actual deflection data.

Selection of appropriate regularization parameter was done by iteration, and visual evaluation of TVDR results against real curvature profiles of deflection models. In simple words, too high values for α yielded “stiff” and inaccurate curvature profiles; meaning that abrupt changes of slope were not recognized, and values of profile were significantly off the range of real curvature values. On the contrary, too low of curvature parameter produced excessive scatter of results; thus a realistic profile cannot be observed

Figure 13 will demonstrate, in plots, what the results from using “too high”, “too low”, and “appropriate” values of α, look like. Furthermore, Appendix D shows a list of regularization parameter values, evaluated through this qualitative criteria; and those considered “appropriate”. Appropriate regularization parameters resulted within $1 \cdot 10^{-12}$ and $1 \cdot 10^{-14}$ range of curvature values; therefore, these were all involved in the TVDR implementation to deflection data.

Equation (15) was used again, along with TVDR result, to determine profiles of substrate curvature change. Similarly to the previous section, average and standard deviation were used to quantify consistency among different regularization parameters; and also, to compare such method with the polynomial fitting method.

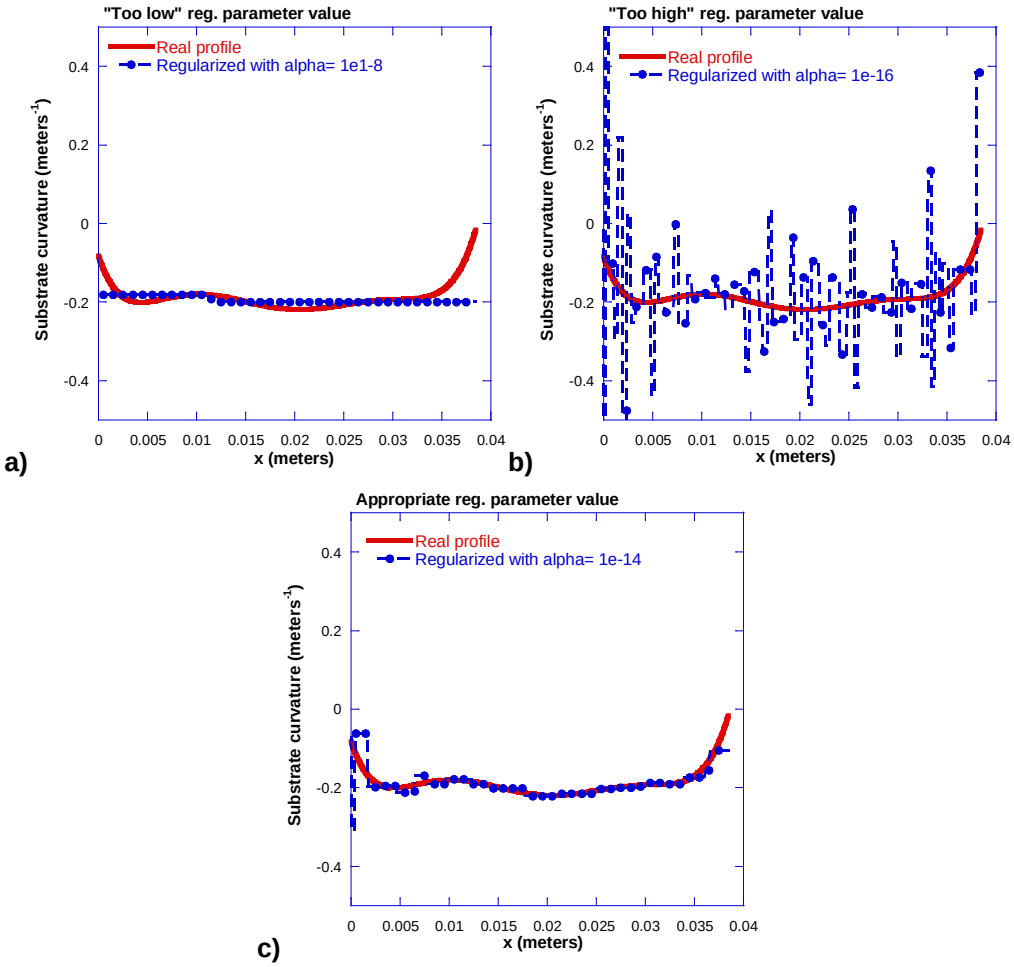

Figure 13. Visual inspection of regularization parameter (*α*) effects, classified as a) too low, b) too high, and c) adequate.

Figure 14 is an example of the average curvature profiles that the TVRD method generated at the 0 and 90° orientations for one of the 3C-SiC on Si systems. Figure 15 shows the exact type of information; but instead, it corresponds to W films on Si (100) substrate combination. Polynomial fitting and segmentation method results are also shown in these figures. Plots in Appendices B and C also show regularization results, facilitating this comparison through direct observation. These appendix sections will aid on the comparison of curvature analysis methods, which is presented in the following section.

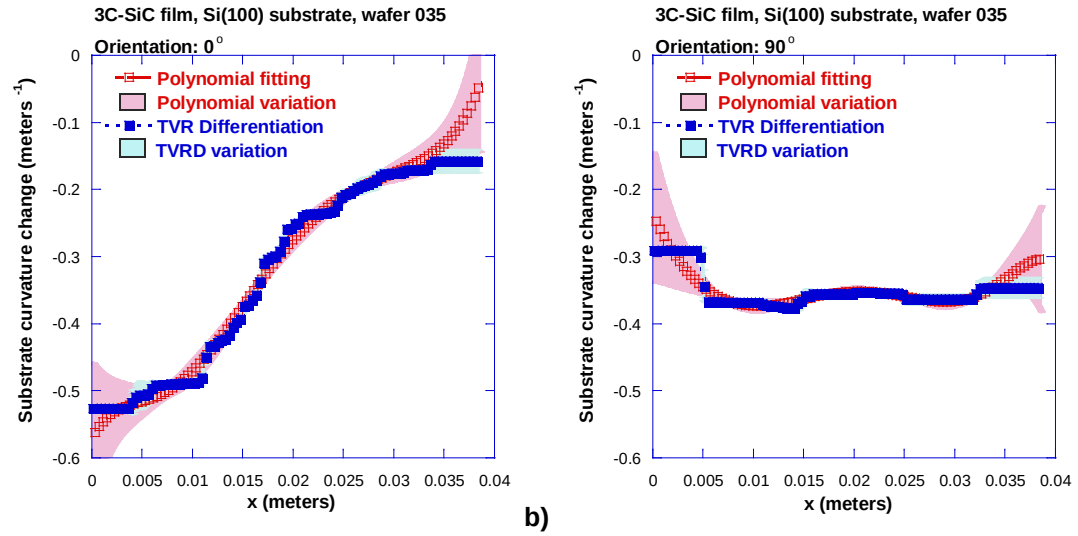

a) b)

Figure 14. Comparison of analysis methods for substrate curvature change of 3C-SiC film on Si (100) along (a) 0° and (b) 90° scan orientations.

TVRD generates curvature change profiles very similar to those derived previously by polynomial fitting; with the same exact trends in both directions. However, amounts of variations in average substrate curvature change are smaller along every profile, indicating a higher consistency of results among the regularization parameters used.

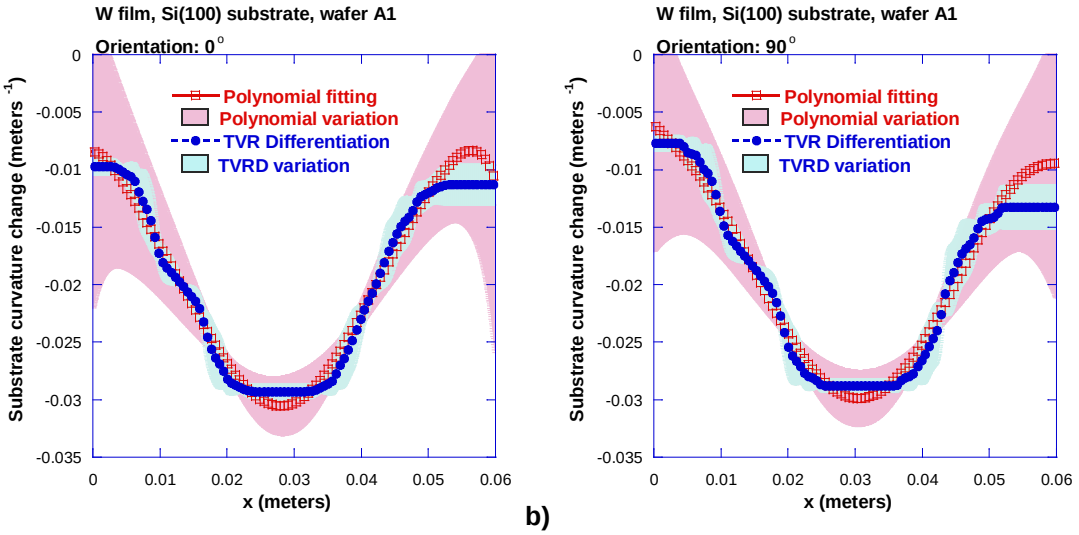

a) b)

Figure 15. Comparison of analysis methods for substrate curvature change of W film on Si (100) along (a) 0° and (b) 90° scan orientations.

A distinguishing trait observed on TVRD results was the “ladder effect”, which consists in small step changes that make any slope in the profile, and was predicted by author of this regularization algorithm [96]. Figure 13, previously shown, reveals how real curvature profiles can be smoother that TVDR resultant profile; meaning that this “ladder effect” should be either removed, or disregarded.

2.5 Comparison of substrate curvature analysis methods

The most noticeable difference between both analysis methods seemed to be in the presence of predefined behavior of polynomial functions. This statement is evidenced over both edges of all curvature profiles substrate scan; and also along the middle segments of the W film on Si substrate data. TVDR results indicated that substrate curvature change remained constant over these segments. On the contrary, large profile abruptions were assumed by polynomial fits over these segments; which were unclear due to significant variation that resulted among different polynomial degrees of fit.

In section 2.2, polynomial behavior was examined in terms of how it becomes more unpredictable as the ends of data domain are approached. Furthermore, polynomials might have excessive degree of freedom to represent center portion of W on Si deflection data, as TVDR oppositely represent these segments as constant curvature sections.

Results from segmentation method are very similar to those produced by polynomial fitting over entire data domain. This method did not show to be much more advantageous than polynomial fitting, mainly because curvature results are discrete, leaving uncertainty about curvature change on locations between segments. The appropriate way on how to determine the surrounding region of possible substrate curvature change is unknown. It was confirmed that if data was divided into more segments than the selected amount of 10, higher residual norm resulted when analyzing data simulation; moreover, segmented curvature profiles would present significant scatter, which is illogical for continuous surfaces. Similar scatter was observed when utilizing a number of segments higher than 10.

In TVDR implementation, there is no dependence on pre-defined function behavior; instead, it “adjusts” each single data point to a desired level of scatter reduction. Selection of a regularization parameter is what adjusts this “reduction”, better called regularization, so that it does not become destructive. The beauty of this comparison is that polynomial fitting is allowed for prior knowledge about the form of substrate curvature profile that can be expected.

While there is a perceptible relation between substrate curvature and deposited film thickness profiles, it is suspected that film thickness generates a residual stress gradient across the body of the film. In the case of 3C-SiC, along 0° oriented substrate diameter, there is a linear increase in film thickness; while there is a decrease in substrate curvature change. On the other hand, 90° orientated profiles do not show such correlation, although symmetrical film

thickness profiles seem to go in hand with apparently symmetrical and almost constant substrate curvature change profiles. Consequently, thickness profile along 0° direction appears to be significant for the resultant, non-uniform substrate curvature.

A probable explanation for resultant non-uniform curvature change is that a film thickness gradient would somehow cause local residual film stress levels to vary across plane of the film. Normal stress gradient together with adhesion bonds at the film-substrate interface would cause shear stresses to arise; hence, a varying internal bending moment would be generated on the substrate.

TVDR results have the advantage of detecting abrupt changes in substrate curvature, which could be generated by either high nature of non-uniform residual film stress. Moreover, regularization does not destroy information at the edges of substrate; for this reason, this analysis method shows favorable for developing a full field curvature measurement technique, which with appropriate numerical implementation, can be related to residual film stress.

Chapter 3.

Conclusions and Future Work

A background about formation mechanisms and measurement of residual thin film stresses has been given with a focus on 3C-SiC films on 100 Si substrates; and the present work has proposed a tool for the development of a more complete residual film stress measurement technique. Regardless of accuracy loss, the substrate curvature method is attractive enough to use it beyond its limitations. Proposed extensions of Stoney's equation require of substrate deflection measurements to determine all substrate curvature components existing along in-plane directions.

Polynomial fitting is not an accurate indicator of substrate curvature change at the substrate edges. Any degree of freedom might be enough to approximate substrate deflection data with negligible difference between measured and modeled results. However, great differences are obtained when the second derivatives of such fits are studied.

Regularization, which is commonly used as an image reconstruction tool, has been proposed here for developing a more appropriate measurement procedure, via mechanical surface profilometry. It was confirmed that TVDR can well approximate real second derivatives from deflection data, which possesses misleading scatter. Selection of regularization parameter shall be based on

accurate expectations about how much scatter does not correspond to actual substrate profile.

Numerical analysis has been developed by several studies in order to expand scope of applications for Stoney's equation. Conclusions from these techniques have settled on the need for measuring full field curvature change of substrate upon thin film deposition. While more complicated optical tools can be developed for such measurements, current mechanical profilometry tools are inexpensive, and simple to use. By using a different procedure, and more powerful method for analysis of deflection data, mechanical profilometry could probably be adjusted to meet the demands of Stoney's equation expansions. TVDR is a potential complement to this development.

Non-uniform, and non-axis symmetric substrate curvatures that were observed on the samples of this work, can be attributed to film thickness non-uniformities. Nevertheless, Stoney's equation was enough to determine with adequate accuracy average residual film stress value at the point at which substrate curvature is equibiaxial. At this location, 0° and 90° oriented curvature change profiles coincide; hence, orthogonal components are equal. The axis symmetric shape of a round substrate contributes for equibiaxial curvature location to be the circumferential center of the substrate. Nevertheless, thickness non-uniformity, crystal structure defects, and wafer flat cause equibiaxial curvature to deviate from such location.

For the purpose of illustrating the equibiaxial stress within the substrate geometry, Stoney's equation was implemented locally, so that $\sigma(x)$ results from

utilizing equation (12) with functions $k(x)$, and $t_f(x)$; which corresponded to the measured profiles presented above. It was clearly noted in Chapter 1 that stress non-uniformities are not accounted for by equation (12); hence, profiles of this nature are inaccurate, except for the single equibiaxial-stress point, at which all orientations coincide. Figure 16 illustrates the equibiaxial film stress point for one of the 3C-SiC film samples. While knowing that non-uniformities can be significant, this single value of equibiaxial stress has been utilized for estimation purposes [97]. Because of having implemented different analysis methods, a certain stress profile was derived from each substrate curvature change result. The rest of equibiaxial stress values for all samples considered are listed on Appendix E.

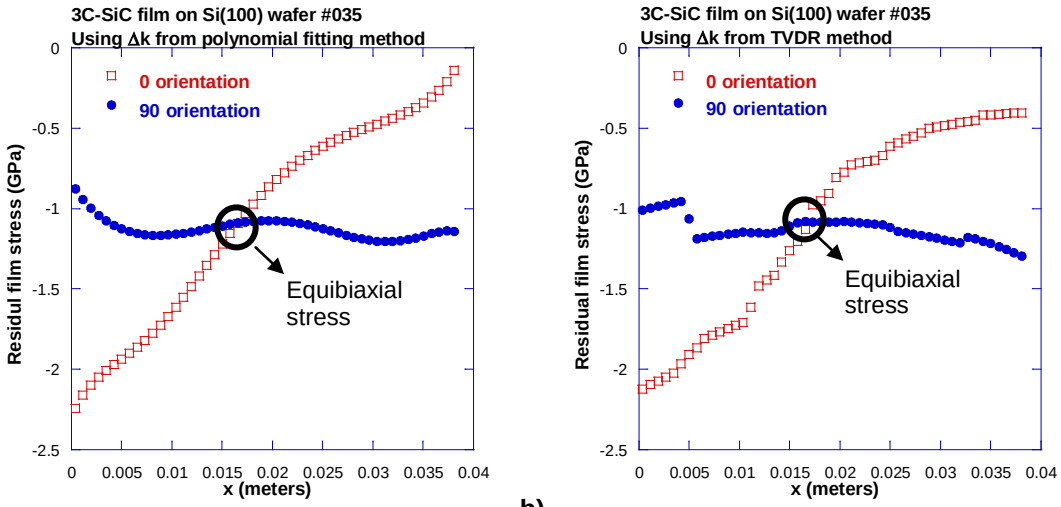

a) b)

Figure 16. Residual film stress profiles after direct implementation of Stoney's equation. Substrate curvature change profiles are those obtained by a) Polynomial fitting, and b) TVDR methods.

Volinsky et al have estimated inaccuracies from using Stoney's equation in this manner by using a correction factor, derived from a finite element model,

based on axis-symmetric, non-uniform substrate curvature and film thickness. [38]. This approach is an example for a temporary solution until proposed next steps are completed.

The next steps of this study shall first include validation of equibiaxial stress results presented above. Furthermore, it is necessary to develop a new measurement procedure, using mechanical profilometry instrument (Tencor P-20 Profilometer) with the goal of providing complete curvature change information across the entire substrate. Because of non-symmetric film thickness profiles are generated upon CVD, new procedure of measurement would require more than few scan lines, orthogonal to each other. Desired result is to obtain more than one component of curvature, and residual film stress could then be determined.

Further understanding of thin, bi-layered plate mechanics is essential to provide appropriate derivation of curvature-stress relations that do not assume limiting conditions, such as thickness uniformity, equibiaxial, uniform curvature and stress components, and anisotropic materials. Numerical analysis shall be complemented by finite element modeling, which confirms obtained results. Moreover, numerical analysis that was referenced in section 2.5 could also be included for validation with finite element modeling.

References

[1] Agarwal, A., and Saddow, S.E., 2004, "Advances in silicon carbide processing and applications," Artech House, Boston, p. 212.

[2] Davis, R. F., Kelner, G., Shur, M., 1991, "Thin Film Deposition and Microelectronic and Optoelectronic Device Fabrication and Characterization in Monocrystalline Alpha and Beta Silicon Carbide," Proceedings of the IEEE, 79(5) pp. 677-701.

[3] Casady, J. B., and Johnson, R. W., 1996, "Status of Silicon Carbide (SiC) as a Wide-Bandgap Semiconductor for High-Temperature Applications: A Review " Solid-State Electronics, 39(10) pp. 1409-1422.

[4] Hefner, A. R., Jr., Singh, R., Jih-Sheg Lai, 2001, "SiC Power Diodes Provide Breakthrough Performance for a Wide Range," IEEE Transactions on Power Electronics pp. 273-280.

[5] Lai, J. - Huang, X., Yu, H., 2001, "High current SiC JBS diode characterization for hard- and soft-switching applications," Industry Applications Conference, 2001. Thirty-Sixth IAS Annual Meeting. Conference Record of the 2001 IEEE, 1 pp. 384-390

[6] Elasser, A., and Chow, T. P., 2002, "Silicon Carbide Benefits and Advantages for Power Electronics Circuits and Systems," Proceedings of the IEEE, 90(6) pp. 969-986.

[7] Spetz, A. L., Unéus, L., Svenningstorp, H., 2001, "SiC Based Field Effect Gas Sensors for Industrial Applications," Physica Status Solidi (a), 185(1) pp. 15-25.

[8] Fawcett, T. J., Wolan, J. T., Lloyd, A., 2006, "Thermal Detection Mechanism of SiC Based Hydrogen Resistive Gas Sensors " Applied Physics Letters, 89(18) p. 182.

[9] Wingbrant, H., 2003, "Using a MISiCFET Device as a Cold Start Sensor " Sensors and Actuators.B, Chemical, 93(1) pp. 295.

[10] Sundararajan, S., and Bhushan, B., 1998, "Micro/nanotribological Studies of Polysilicon and SiC Films for MEMS Applications," Wear, 217(2) pp. 251-261.

[11] Reddy, J. D., Volinsky, A. A., Frewin, C. L., 2008, "Mechanical properties of 3C-SiC films for MEMS applications " Proceedings Materials Research Society, Warrendale, PA, USA, 1049 p. 41.

[12] Fisher, G. R., and Barnes, P., 1990, "Towards a Unified View of Polytypism in Silicon Carbide " Philosophical Magazine.B, Physics of Condensed Matter, Electronic, Optical, and Magnetic Properties, 61(2) p. 217.

[13] Jacobson, H., Birch, J., Yakimova, R., 2002, "Dislocation Evolution in 4H-SiC Epitaxial Layers," Journal of Applied Physics, 91(10) pp. 6354-6360.

[14] Janzén, E., Son, N. T., Magnusson, B., 2006, "Intrinsic Defects in High-Purity SiC," Microelectronic Engineering, 83(1) pp. 130-134.

[15] Nishino, S., 1983, "Production of Large-Area Single-Crystal Wafers of Cubic SiC for Semiconductor Devices " Applied Physics Letters, 42(5) p. 460.

[16] Powell, A. R., and Rowland, L. B., 2002, "SiC Materials-Progress, Status, and Potential Roadblocks " Proceedings of the IEEE, 90(6) p. 942.

[17] Vinod, K., Zorman, C., Yasseen, A., 1998, "Fabrication of Low Defect Density 3C-SiC on SiO2 Structures using Wafer Bonding Techniques " Journal of Electronic Materials, 27(3) pp. L17-L20.

[18] Harada, S., 2004, "Uniformity Improvement in SiC Epitaxial Growth by using Si-Condensation," Materials Science Forum, 457 p. 225.

[19] Nishio, J., Hasegawa, M., Kojima, K., 2003, "Uniformity of 4H–SiC Epitaxial Layers Grown on 3-in Diameter Substrates," Journal of Crystal Growth, 258(1-2) pp. 113-122.

[20] Konstantinov, A. O., Hallin, C., Pécz, B., 1997, "The Mechanism for Cubic SiC Formation on Off-Oriented Substrates," Journal of Crystal Growth, 178(4) pp. 495-504.

[21] Nordell, N., Anderson, S. G., and Schoner, A., 1996, "A new reactor concept for epitaxial growth of SiC " Silicon Carbide and Related Materials 1995. Proceedings of the Sixth International Conference. S. Nakashima and H. Matsunami, eds. IOP Publishing, Bristol, UK, pp. 81-84.

[22] Wu, C. H., Jacob, C., Ning, X. J., 1996, "Epitaxial growth of single crystalline 3C-SiC on Si from hexamethyldisilane and void formation mechanism " Silicon Carbide and Related Materials 1995. Proceedings of the Sixth International Conference. S. Nakashima and H. Matsunami, eds. IOP Publishing, Bristol, UK, pp. 97-100.

[23] Hirai, M., Miyatake, M., Kusaka, M., 1996, "PECVD growth of a-$Si_{1-x}C_x$:H thin film on Si(111) substrates by ion species " Silicon Carbide and Related Materials 1995. Proceedings of the Sixth international Conference. S. Nakashima and H. Matsunami, eds. IOP Publishing, Bristol, UK, pp. 1043-1046.

[24] Wickramanayaka, S., Kitamura, K., Nakanishi, Y., 1996, "Chemical and mechanical properties of a-SiC:H films deposited in remote hydrogen plasma using hexamethyldisilane as the source monomer " Silicon Carbide and Related Materials 1995. Proceedings of the Sixth International Conference S. Nakashima and H. Matsunami, eds. IOP Publishing, Bristol, UK, pp. 1051-1054.

[25] Sato, S., Mizushima, I., Miyano, K., 2005, "Defects Induced by Carbon Contamination in Low-Temperature Epitaxial Silicon Films Grown with Monosilane " Japanese Journal of Applied Physics, 44(3) p. 1169.

[26] Chung, H. J., Polyakov, A. Y., Huh, S. W., 2005, "Bulk Growth of High-Purity 6H-SiC Single Crystals by Halide Chemical-Vapor Deposition " Journal of Applied Physics, 97(8) p. 1.

[27] Yakimova, R., and Janzén, E., 2000, "Current Status and Advances in the Growth of SiC " Diamond and Related Materials, 9(3-6) pp. 432-438.

[28] Ishida, Y., 2009, "Development of a Practical High-Rate CVD System " Materials Science Forum, 600 p. 119.

[29] Zhang, J., Forsberg, U., Isacson, M., 2002, "Growth Characteristics of SiC in a Hot-Wall CVD Reactor with Rotation," Journal of Crystal Growth, 241(4) pp. 431-438.

[30] Mehregany, M., and Zorman, C. A., 1999, "SiC MEMS: Opportunities and Challenges for Applications in Harsh Environments," Thin Solid Films, 355-356 pp. 518-524.

[31] Jackson, K. M., Dunning, J., Zorman, C. A., 2005, "Mechanical Properties of Epitaxial 3C Silicon Carbide Thin Films," Microelectromechanical Systems, Journal of, 14(4) pp. 664-672.

[32] Stoney, G. G., 1909, "Tension of Electro-Deposited Films," Proceedings of the Royal Society of London, 82 p. 172.

[33] Nix, W., 1989, "Mechanical Properties of Thin Films," Metallurgical Transactions.A, Physical Metallurgy and Materials Science, 20(11) p. 2217.

[34] Doerner, M., and Nix, W. D., 1988, "Stresses and Deformation Processes in Thin Films on Substrates " Critical Reviews in Solid State and Materials Sciences, 14(3) p. 225.

[35] Withers, P. J., and Bhadeshia, H. K. D. H., 2001, "Residual Stress. 2. Nature and Origins," Materials Science and Technology MST, 17(4) pp. 366-375.

[36] Suo, Z., and Hutchinson, J. W., 1989, "Steady-State Cracking in Brittle Substrates Beneath Adherent Films," International Journal of Solids and Structures, 25(11) pp. 1337-1353.

[37] Evans, A. G., Drory, M. D., and Hu, M. S., 1988, "Cracking and Decohesion of Thin Films " Journal of Materials Research, 3(5) p. 1043.

[38] Volinsky, A. A., Kravchenko, G., Waters, P., 2008, "Residual stress in CVD-grown 3C-SiC films on Si substrates," Silicon Carbide 2008 - Materials, Processing and Devices, Anonymous Materials Research Society, Warrendale, PA 15086, United States, 1069, pp. 109-114.

[39] Lu, Y. M., and Leu, I. C., 2000, "Qualitative Study of Beta Silicon Carbide Residual Stress by Raman Spectroscopy," Thin Solid Films, 377-378 pp. 389-393.

[40] Fu, X., Dunning, J. L., Zorman, C. A., 2005, "Measurement of Residual Stress and Elastic Modulus of Polycrystalline 3C-SiC Films Deposited by Low-Pressure Chemical Vapor Deposition," Thin Solid Films, 492(1-2) pp. 195-202.

[41] Roy, S., Zorman, C., Mehregany, M., 2006, "The Mechanical Properties of Polycrystalline 3C-SiC Films Grown on Polysilicon Substrates by Atmospheric Pressure Chemical-Vapor Deposition " Journal of Applied Physics, 99(4) p. 44108.

[42] Zhu, W. L., Zhu, J. L., Nishino, S., 2006, "Spatially Resolved Raman Spectroscopy Evaluation of Residual Stresses in 3C-SiC Layer Deposited on Si Substrates with Different Crystallographic Orientations," Applied Surface Science, 252(6) pp. 2346-2354.

[43] Lin, T. Y., Duh, J. G., Chung, C. K., 2000, "Fabrication of Low-Stress Plasma Enhanced Chemical Vapor Deposition Silicon Carbide Films " Japanese Journal of Applied Physics, 39(12) p. 6663.

[44] Fu, X., Dunning, J. L., Zorman, C. A., 2005, "Polycrystalline 3C-SiC Thin Films Deposited by Dual Precursor LPCVD for MEMS Applications " Sensors and Actuators A: Physical, 119(1) pp. 169-176.

[45] Withers, P. J., 2001, "Residual Stress. 1. Measurement Techniques " Materials Science and Technology MST, 17(4) p. 355.

[46] Malhotra, S. G., Rek, Z. U., Yalisove, S. M., 1997, "Analysis of Thin Film Stress Measurement Techniques," Thin Solid Films, 301(1-2) pp. 45-54.

[47] Bunshah, R.F., McGuire, G.E., and Schuegraf, K.K., 1988, "Handbook of thin-film deposition processes and techniques : principles, methods, equipment, and applications," Noyes Publications, Park Ridge, N.J., U.S.A., p. 413.

[48] Noyan, I. C., 1995, "Residual stress/strain Analysis in Thin Films by x-Ray Diffraction," Critical Reviews in Solid State and Materials Sciences, 20(2) p. 125.

[49] Cullity, B.D., 1978, "Elements of X-ray diffraction, 2nd edition," Addison Wesley series in metallurgy and materials.

[50] Gelfi, M., Bontempi, E., Roberti, R., 2004, "Residual Stress Analysis of Thin Films and Coatings through XRD2 Experiments," Thin Solid Films, 450(1) pp. 143-147.

[51] Zheng, X. J., Yang, Z. Y., and Zhou, Y. C., 2003, "Residual Stresses in Pb(Zr0.52Ti0.48)O3 Thin Films Deposited by Metal Organic Decomposition," Scripta Materialia, 49(1) pp. 71-76.

[52] McCandless, B.E., 2005, "Glancing incidence X-ray diffraction of polycrystalline thin films," Thin Film Compound Semiconductor Photovoltaics, San Francisco, CA, pp. 75-86.

[53] Tang, W., Deng, L., Xu, K., 2007, "X-Ray Diffraction Measurement of Residual Stress and Crystal Orientation in Au/NiCr/Ta Films Prepared by Plating," Surface and Coatings Technology, 201(12) pp. 5944-5947.

[54] Malhotra, S. G., 1996, "Depth Dependence of Residual Strains in Polycrystalline Mo Thin Films using High-Resolution X-Ray Diffraction," Journal of Applied Physics, 79(9) p. 6872.

[55] Malhotra, S. G., 1997, "Strain Gradients and Normal Stresses in Textured Mo Thin Films," Journal of Vacuum Science Technology.A.Vacuum, Surfaces, and Films, 15(2) p. 345.

[56] Zhang, S., Xie, H., Zeng, X., 1999, "Residual Stress Characterization of Diamond-Like Carbon Coatings by an X-Ray Diffraction Method," Surface and Coatings Technology, 122(2-3) pp. 219-224.

[57] Rohmfeld, S., 2000, "Raman Spectroscopy on Biaxially Strained Epitaxial Layers of 3C-SiC on Si," Materials Science Forum, 338(1) p. 595.

[58] Feng, Z. C., 1988, "Raman Determination of Layer Stresses and Strains for Heterostructures and its Application to the Cubic SiC/Si System," Journal of Applied Physics, 64(12) p. 6827.

[59] Veprek, S., 1997, "Relaxation of Interfacial Stress and Improved Quality of Heteroepitaxial 3C-SiC Films on (100)Si Deposited by Organometallic Chemical Vapor Deposition at 1200 Deg C," Journal of Vacuum Science Technology.A.Vacuum, Surfaces, and Films, 15(1) p. 10.

[60] Amer, M. S., Durgam, L., and El-Ashry, M. M., 2006, "Raman Mapping of Local Phases and Local Stress Fields in silicon–silicon Carbide Composites," Materials Chemistry and Physics, 98(2-3) pp. 410-414.

[61] Shao, S., Fan, Z., Shao, J., 2003, "Evolutions of Residual Stress and Microstructure in ZrO2 Thin Films Deposited at Different Temperatures and Rates," Thin Solid Films, 445(1) pp. 59-62.

[62] Cuthrell, R. E., 1988, "Residual Stress Anisotropy, Stress Control, and Resistivity in Post Cathode Magnetron Sputter Deposited Molybdenum Films," Journal of Vacuum Science Technology.A.Vacuum, Surfaces, and Films, 6(5) p. 2914.

[63] Thornton, J. A., 1985, "The Influence of Discharge Current on the Intrinsic Stress in Mo Films Deposited using Cylindrical and Planar Magnetron Sputtering Sources," Journal of Vacuum Science Technology.A.Vacuum, Surfaces, and Films, 3(3) p. 576.

[64] Himes, J., 2001, "Effect of Externally-Imposed Radial Strain on the Piezoelectric Response of MOCVD-Grown Gallium Nitride," Materials Research Society Symposia Proceedings, 639 p. G11.

[65] Yi, J. W., Lee, Y. H., and Farouk, B., 2000, "Low Dielectric Fluorinated Amorphous Carbon Thin Films Grown from C6F6 and Ar Plasma," Thin Solid Films, 374(1) pp. 103-108.

[66] Adams, D. P., Parfitt, L. J., Bilello, J. C., 1995, "Microstructure and Residual Stress of very Thin Mo Films," Thin Solid Films, 266(1) pp. 52-57.

[67] Kuo, C. L., 1984, "Residual strains in amorphous silicon films measured by X-ray double crystal topography" Journal of Applied Physics, 55(2) p. 375.

[68] Tao, J., 1991, "Non-Destructive Evaluation of Residual Stresses in Thin Films Via X-Ray Diffraction Topography Methods," Journal of Electronic Materials, 20(10) p. 819.

[69] Costa, M. F. M., 2001, "Thin Films' Residual Stress Measurement by Optical Profilometry," Proceedings of SPIE--the International Society for Optical Engineering, 4596 p. 1.

[70] Waters, P., 2008, "Stress Analysis and Mechanical Characterization of Thin Films for Microelectronics and MEMS Applications." PhD Dissertation, University of South Florida, Tampa, Fl

[71] Rosakis, A. J., Singh, R. P., Tsuji, Y., 1998, "Full Field Measurements of Curvature using Coherent Gradient Sensing: Application to Thin Film Characterization," Thin Solid Films, 325(1-2) pp. 42-54.

[72] Ngo, D., Feng, X., Huang, Y., 2007, "Thin film/substrate Systems Featuring Arbitrary Film Thickness and Misfit Strain Distributions. Part I: Analysis for Obtaining Film Stress from Non-Local Curvature Information," International Journal of Solids and Structures, 44(6) pp. 1745-1754.

[73] Freund, L.B., and Suresh, S., 2003, "Thin film materials : stress, defect formation and surface evolution," Cambridge University Press, Cambridge, England ; New York, p. 750.

[74] Wikström, A., Gudmundson, P., and Suresh, S., 1999, "Thermoelastic Analysis of Periodic Thin Lines Deposited on a Substrate," Journal of the Mechanics and Physics of Solids, 47(5) pp. 1113-1130.

[75] Wikstrom, A., Gudmundson, P., and Suresh, S., 1999, "Analysis of Average Thermal Stresses in Passivated Metal Interconnects," Journal of Applied Physics, 86(11) pp. 6088-6095.

[76] Shen, Y. -., Suresh, S., and Blech, I. A., 1996, "Stresses, Curvatures, and Shape Changes Arising from Patterned Lines on Silicon Wafers," Journal of Applied Physics, 80(3) pp. 1388-1398.

[77] Masters, C. B., and Salamon, N. J., 1993, "Geometrically Nonlinear Stress-Deflection Relations for Thin film/substrate Systems," International Journal of Engineering Science, 31(6) pp. 915-925.

[78] Salamon, N. J., and Masters, C. B., 1995, "Bifurcation in Isotropic thinfilm/substrate Plates," International Journal of Solids and Structures, 32(3-4) pp. 473-481.

[79] Finot, M., Blech, I. A., Suresh, S., 1997, "Large Deformation and Geometric Instability of Substrates with Thin-Film Deposits," Journal of Applied Physics, 81(8) pp. 3457-3464.

[80] Freund, L. B., 2000, "Substrate Curvature due to Thin Film Mismatch Strain in the Nonlinear Deformation Range " Journal of the Mechanics and Physics of Solids, 48(6-7) pp. 1159-1174.

[81] Park, T. -., and Suresh, S., 2000, "Effects of Line and Passivation Geometry on Curvature Evolution during Processing and Thermal Cycling in Copper Interconnect Lines," Acta Materialia, 48(12) pp. 3169-3175.

[82] Lee, H., Rosakis, A. J., and Freund, L. B., 2001, "Full-Field Optical Measurement of Curvatures in Ultra-Thin-Film--Substrate Systems in the Range of Geometrically Nonlinear Deformations," Journal of Applied Physics, 89(11) pp. 6116-6129.

[83] Volinsky, A. A., Hauschildt, M., Vella, J. B., 2002, "Residual stress and microstructure of electroplated Cu film on different barrier layers " Materials Research Society, Warrendale, PA, USA, 695, pp. 27-32.

[84] Huang, Y., and Rosakis, A. J., 2005, "Extension of Stoney's Formula to Non-Uniform Temperature Distributions in Thin film/substrate Systems. the Case of Radial Symmetry," Journal of the Mechanics and Physics of Solids, 53(11) pp. 2483-2500.

[85] Huang, Y., Ngo, D., and Rosakis, A. J., 2005, "Non-Uniform, Axisymmetric Misfit Strain: In Thin Films Bonded on Plate substrates/substrate Systems: The Relation between Non-Uniform Film Stresses and System Curvatures," Acta Mechanica Sinica, 21(4) pp. 362-370.

[86] Ngo, D., Huang, Y., Rosakis, A. J., 2006, "Spatially Non-Uniform, Isotropic Misfit Strain in Thin Films Bonded on Plate Substrates: The Relation between Non-Uniform Film Stresses and System Curvatures," Thin Solid Films, 515(4) pp. 2220-2229.

[87] Feng, X., Huang, Y., Jiang, H., 2006, "The Effect of Thin Film/Substrate Radii on the Stoney Formula for Thin Film/Substrate Subjected to Nonuniform Axissymmetric Misfit Strain and Temperature " Journal of Mechanics of Materials and Structures, 1(6) pp. 1-16.

[88] Brown, M. A., Rosakis, A. J., Feng, X., 2007, "Thin film/substrate Systems Featuring Arbitrary Film Thickness and Misfit Strain Distributions. Part II: Experimental Validation of the Non-Local stress/curvature Relations," International Journal of Solids and Structures, 44(6) pp. 1755-1767.

[89] Smith, M.T., 2003, "Design and development of a silicon carbide chemical vapor deposition reactor," University of South Florida, Tampa, Fl.

[90] Bakushinskiĭ, A.B., and Goncharskiĭ, A.V., 1994, "Ill-posed problems: theory and applications," Kluwer Academic Publishers, Dordrecht ; Boston, MA.

[91] Murphy, M. C., and Mann, R. W., 1987, "A comparison of smoothing and digital filtering/differentiation of kinematic data " Proceedings of the Ninth Annual Conference of the IEEE Engineering in Medicine and Biology Society IEEE, New York, NY, USA, 2, p. 852.

[92] Gazzani, F., 1994, "Comparative Assessment of some Algorithms for Differentiating Noisy Biomechanical Data " International Journal of Biomedical Computing, 37(1) p. 57.

[93] Tikhonov, A.N., Gonscharsky, A.V., Stepanov, V.V., 1995, "Numerical methods for the solution of ill-posed problems " Kluwer Academic Publishers, Dordrecht ; Boston, p. 253.

[94] Cullum, J., 1971, "Numerical Differentiation and Regularization " SIAM Journal on Numerical Analysis, 8(2) p. 254.

[95] Rudin, L. I., Osher, S., and Fatemi, E., 1992, "Nonlinear Total Variation Based Noise Removal Algorithms," Physica D: Nonlinear Phenomena, 60(1-4) p. 259-268.

[96] Chartrand, R., 2007, "Numerical differentiation of noisy, nonsmooth data " LA-UR-05-9309.

[97] Zhao, Z. B., Hershberger, J., Yalisove, S. M., 2002, "Determination of Residual Stress in Thin Films: A Comparative Study of X-Ray Topography Versus Laser Curvature Method," Thin Solid Films, 415(1-2) pp. 21-31.

Appendices

Appendix A. Substrate curvature results for 3C-SiC films on Si (100) substrates.

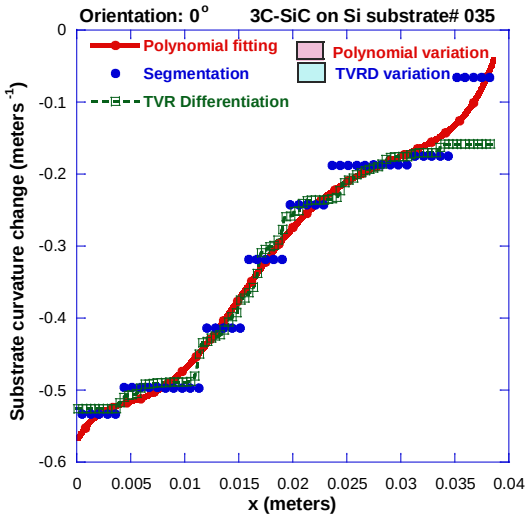

Figure 17. Δκ of sample 035 from 0° scan.

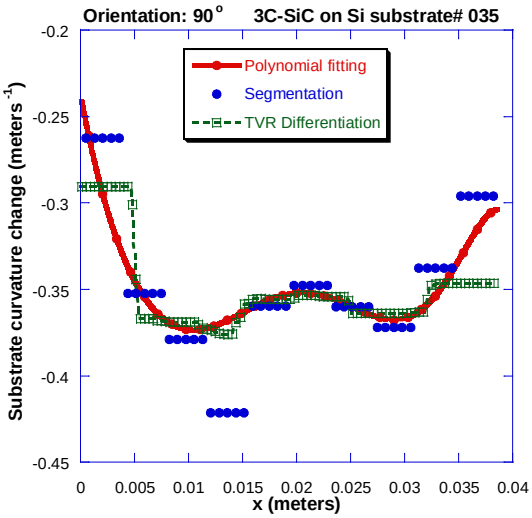

Figure 18. Δκ of sample 035 from 90° scan.

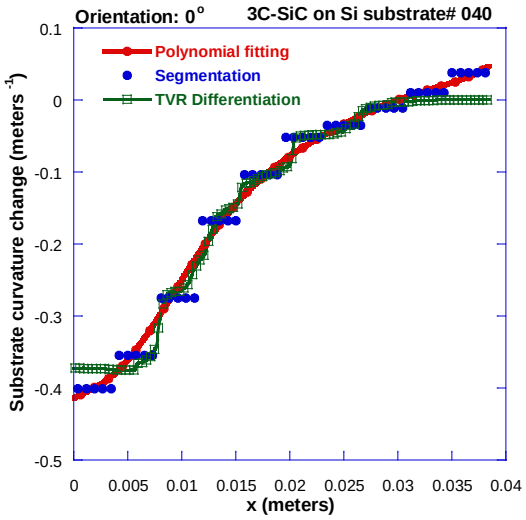

Figure 19. Δκ of sample 040 from 0° scan.

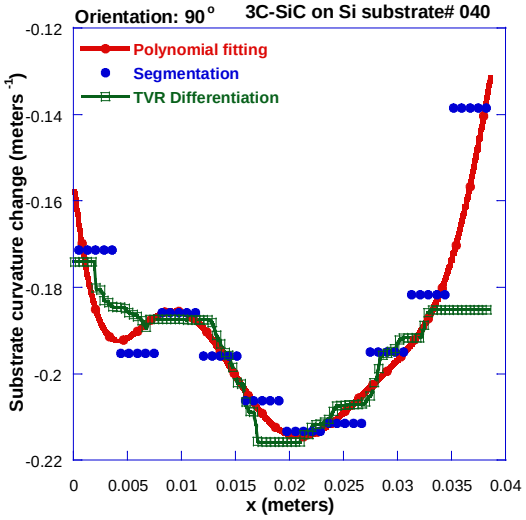

Figure 20. Δκ of sample 040 from 90° scan.

Appendix A. (Continued)

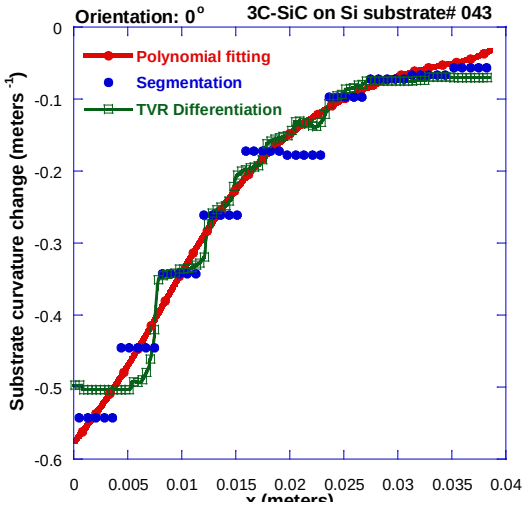

Figure 21. Δκ of sample 043 from 0° scan.

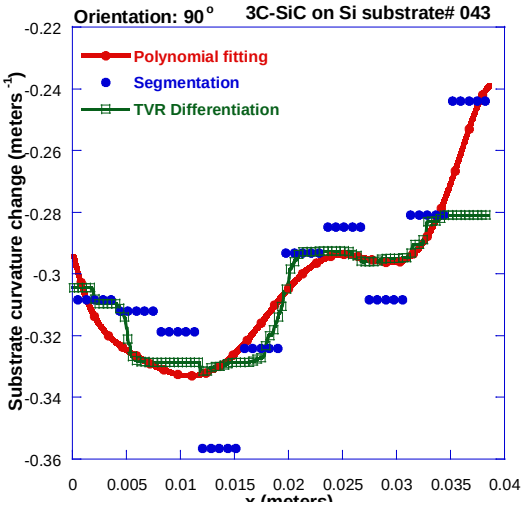

Figure 22. Δκ of sample 043 from 90° scan.

Appendix B. Substrate curvature results for W films on Si (100) substrates.

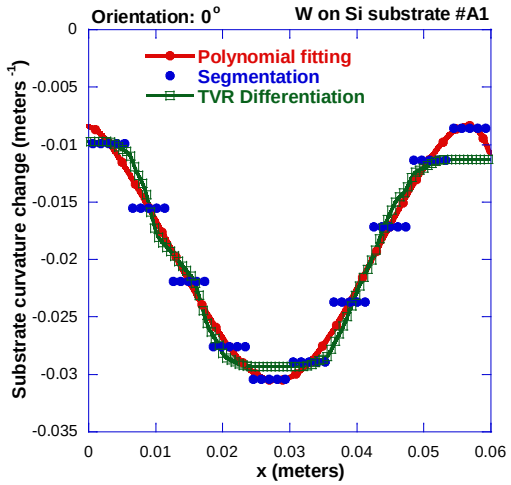

Figure 23. Δκ of sample A1 from 0° scan.

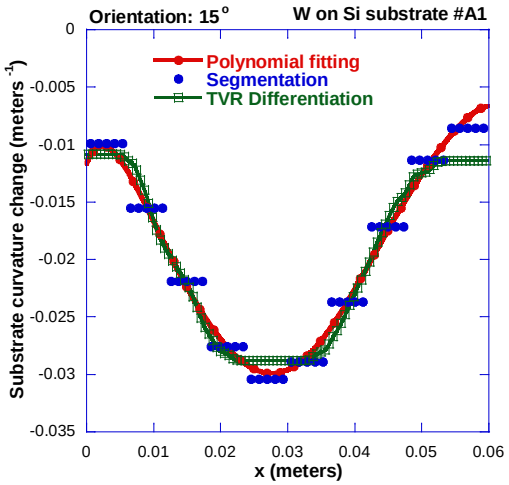

Figure 24. Δκ of sample A1 from 15° scan.

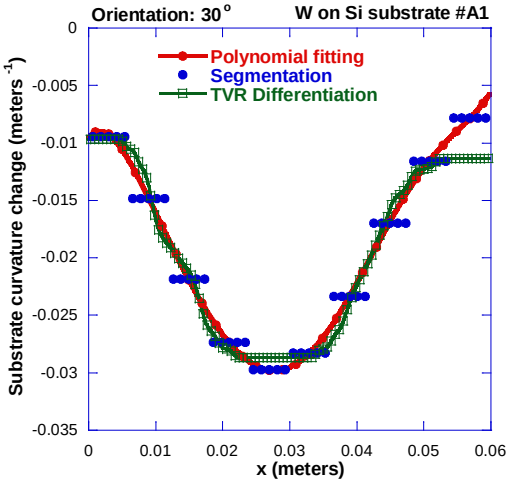

Figure 25. Δκ of sample A1 from 30° scan

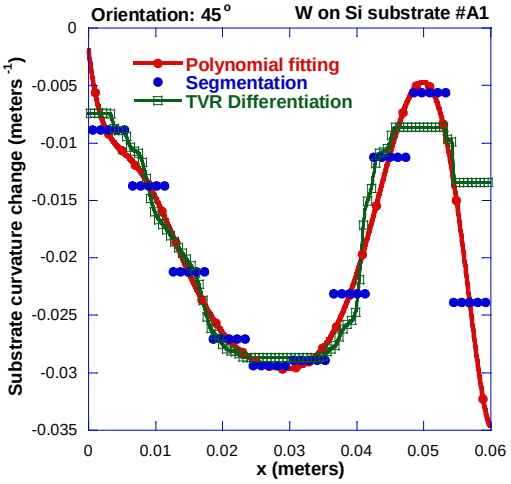

Figure 26. Δκ of sample A1 from 45° scan

Appendix B. (Continued)

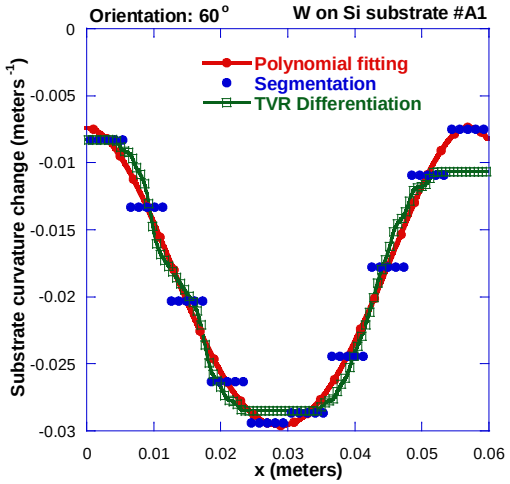

Figure 27. Δκ of sample A1 from 60° scan.

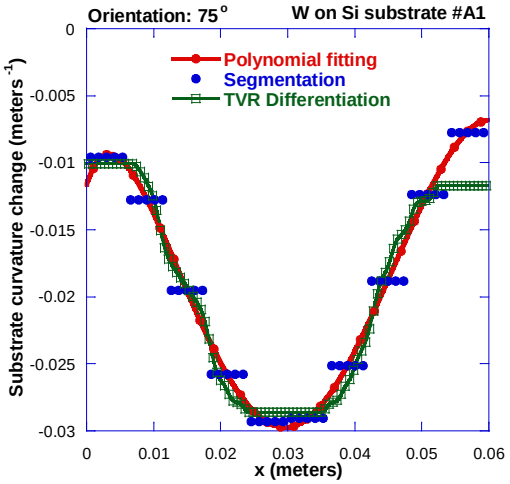

Figure 28. Δκ of sample A1 from 75° scan.

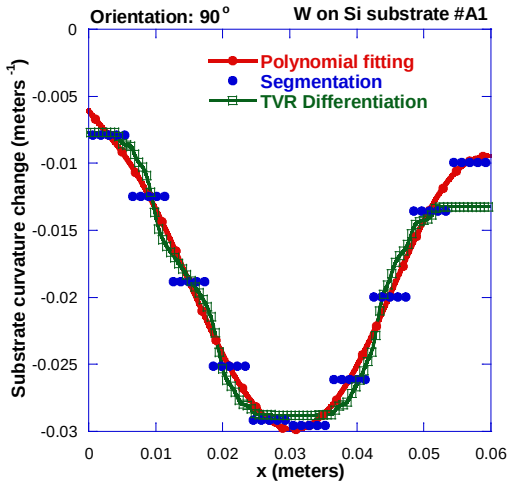

Figure 29. Δκ of sample A1 from 90° scan.

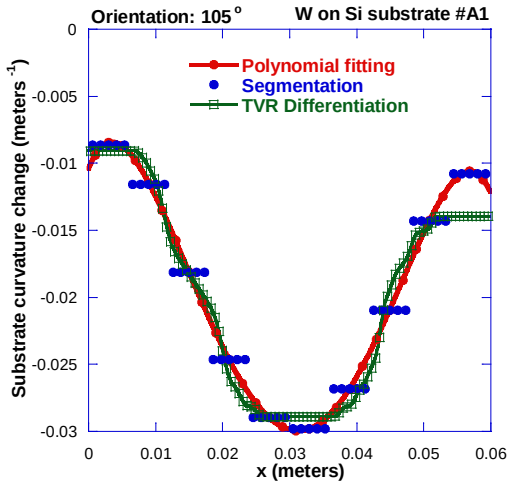

Figure 30. Δκ of sample A1 from 105° scan.

Appendix B. (Continued)

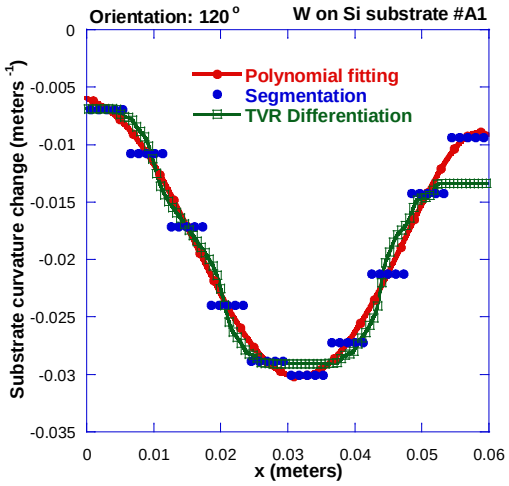

Figure 31. Δκ of sample A1 from 120° scan

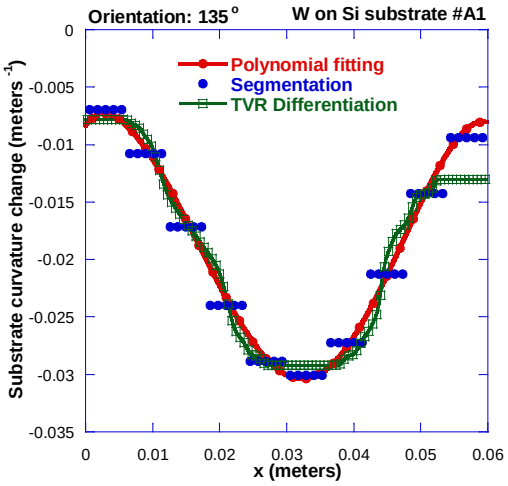

Figure 32. Δκ of sample A1, 135° scan.

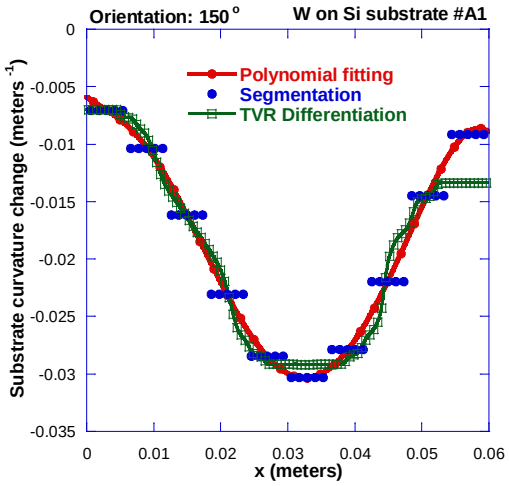

Figure 33. Δκ of sample A1, 150° scan.

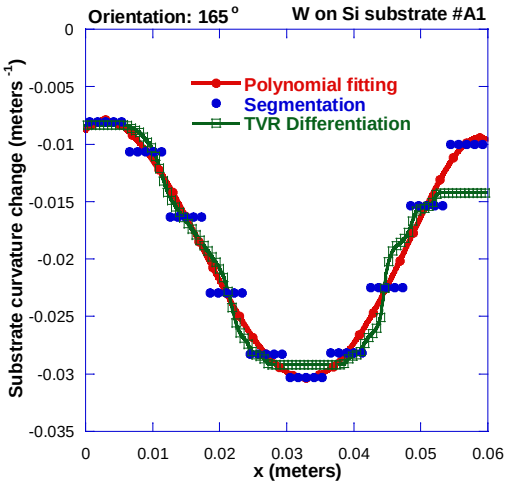

Figure 34. Δκ of sample A1, 165° scan.

Appendix C. Total Variation Regularized Differentiation code using Matlab

Code is modified from original for the purpose of determining regularized second derivative of a data vector [95]. Matlab code is presented below.

```
% tvdiffscp.m: total-variation regularized differentiation
%
% Presumed input: vector e of noisy data to be differentiated.  The
% code assumes that e gives the values of a function at halfway between
% the points of a uniform grid.
%
% Created output: column vector u, regularized derivative of e, given
% at the grid points, so length(u)=length(e)+1.

x=A1rotatedCHANGE(:,1);
y=A1rotatedCHANGE(:,1);

% parameters:
dx=x(2)-x(1); % grid spacing
eps=0.000001; % constant used to avoid division by zero when u' = 0.

% The code seems to tolerate very small values.  Smaller values gets
more accurate results, but slows convergence. Too small makes code
unstable.

alph=1e-10; % regularization parameter.
e=y;
n=size(e,1);

% construct operators of differentiation (D) and antidifferentiation(K)
D=diag(ones(1,n+1))-diag(ones(1,n),-1); %ADJUSTED FROM ORIGINAL
D=[zeros(n+1,1),D];
D(1,1)=-1;
D=D/dx;
K=[zeros(n,1),zeros(n,1)+3/4,zeros(n,n)+0.25*eye(n)];
for i=1:n-1
        K=K+[zeros(n,2),[zeros(i,n);tril(ones(n-i,n-i)),zeros(n-i,i)]];
        K(i+1,2)=K(i+1,2)+i;
        K(i,1)=0.5*i;
end
clear i
K=K*(dx)^2; % Second Integral

% stopping criterion; when change in K*u is less than quit
quit=1e-6;
k=1000;

% initialize to naive derivative
u=[0;0;0;diff(diff(e));0]./dx^2; %%ADJUSTED FROM ORIGINAL
```

Appendix C. (Continued)

```
% since K*u(0)=0, we need to adjust
ofst=e(1);

%while k>quit
for i=1:600
        % solve lagged diffusivity equation.  Alternate dg seems to give
        better results sometimes, for unknown reasons.

        dg=diag(1./sqrt(((u(2:(n+2))-u(1:n+1))/dx).^2+eps));
        % dg=diag(1./sqrt(((u(2:(n+1))-u(1:n))).^2+eps));
        L=dx*D'*dg*D;
        g=K'*(K*u-e+ofst)+alph*L*u;
        H=K'*K+alph*L;
        s=-H\g;
        u=u+s;
        % check stopping condition
        k=norm((*s));
        figure(9),plot(u,'ok'),drawnow;

end
```

Appendix D. Qualitative selection of appropriate regularization parameter (α) values

The different models that were used for this selection process were described in terms of the polynomial degree used, and the SNR of the added Gaussian noise. The following table helps to visualize results that concluded on which regularization parameter values to select.

Table 1. Selection of appropriate regularization parameter by visual inspection criteria.

α ↓ / Model →	Model 1 (8^{th} order / SNR= $1 \cdot 10^6$)	Model 2 (8^{th} order / SNR= $4 \cdot 10^6$)	Model 3 (30^{th} order / SNR= $1 \cdot 10^6$)	Model 4 (30^{th} order / SNR= $4 \cdot 10^6$)
$1 \cdot 10^{-10}$	"Too low"	"Too low"	"Too low"	"Too low"
$1 \cdot 10^{-11}$	"Too low"	"Too low"	"Too low"	"Too low"
$1 \cdot 10^{-12}$	Appropriate	Appropriate	Appropriate	Appropriate
$1 \cdot 10^{-13}$	Appropriate	Appropriate	Appropriate	Appropriate
$1 \cdot 10^{-14}$	Appropriate	Appropriate	Appropriate	Appropriate
$1 \cdot 10^{-15}$	"Too low"	"Too low"	"Too low"	"Too low"
$1 \cdot 10^{-16}$	"Too low"	"Too low"	"Too low"	"Too low"

Appendix E. Local implementation of Stoney's equation with substrate curvature results for 3C-SiC film on Si(100) substrate samples.

Table 2. Magnitude and location of equibiaxial residual stress values.

Sample	Equibiaxial stress using local Stoney's equation and Δk from polynomial fitting method	Equibiaxial stress value using local Stoney's equation and Δk from TVDR method
3C-SiC film on Si (100) wafer# 035	σ (0. 016550 m)= -1.091 GPa	σ(0.016727 m)= -1.082 GPa
3C-SiC film on Si (100) wafer# 040	σ (0. 013117 m)= -0.736 GPa	σ (0.012947 m)= -0.719 GPa
3C-SiC film on Si (100) wafer# 043	σ (0. 010803 m)= -1.215 GPa	σ (0.012127 m)= -1.194 GPa